Title
THE HIGH-ENERGY CHARGED PARTICLES FROM TARGETS BOMBARDED BY 190 MEV DEUTERONS

Author
Schecter, Larry.

Publication Date
1952-10-28

UNIVERSITY OF CALIFORNIA

Radiation Laboratory

BERKELEY, CALIFORNIA

DISCLAIMER

UCRL-1996
Unclassified-Physics Distribution

UNIVERSITY OF CALIFORNIA

Radiation Laboratory

Contract No. W-7405-eng-48

THE HIGH-ENERGY CHARGED PARTICLES FROM TARGETS BOMBARDED BY 190 MEV DEUTERONS

Larry Schecter

(Thesis)

October 28, 1952

Berkeley, California

TABLE OF CONTENTS

TABLE OF CONTENTS

THE HIGH-ENERGY CHARGED PARTICLES FROM TARGETS BOMBARDED BY 190 MEV DEUTERONS

Larry Schecter

Radiation Laboratory, Department of Physics
University of California, Berkeley, California

October 28, 1952

I ABSTRACT

An investigation has been made of the angle and energy distributions of the high energy charged particles which emerge from beryllium, carbon, and uranium nuclei bombarded by 190 Mev deuterons. The results indicate that the yields can be explained as primarily due to two kinds of processes; nucleon-nucleon interactions, and stripping. Under this assumption, the total stripping cross section has been determined to be 0.35 ± 0.03 barns for the lighter elements and 2.6 ± 0.4 barns for uranium. These values suggest an $A^{2/3}$ dependence for this cross section.

THE HIGH-ENERGY CHARGED PARTICLES FROM TARGETS BOMBARDED BY 190 MEV DEUTERONS

Larry Schecter

Radiation Laboratory, Department of Physics
University of California, Berkeley, California

October 28, 1952

II INTRODUCTION

The principal features of the inelastic processes which can be expected to occur, when nuclei are bombarded by high energy deuterons, have been described by the mechanisms of Bohr,[1] Serber,[2] Dancoff,[3] Goldberger,[4] Chew and Goldberger,[5] and Butler[6]. These features concern the various secondary particles whose angular and energy distributions are characteristic of the process which produces them. For deuterons whose incident energy is high, compared to the binding energy, it is convenient to consider a very loosely-bound neutron-proton system. The effects to be described are then merely the results of high energy collisions of nucleons with the nucleus, modified by the relationship of the incident deuteron's constituent nucleons to each other.

When the incident nucleons have energy less than, roughly, 30 to 40 Mev, (corresponding to an incident deuteron energy of less than 70 to 80 Mev, since the total energy is shared equally, on the average) the compound nucleus of Bohr describes one process. In this model, the mean free path of either incident nucleon within the nucleus is so short that its energy is quickly shared with other constituents

of the nucleus, so that it is immediately captured. The resulting excited nucleus decays slowly, either by quantum emission, or, when sufficient energy becomes concentrated properly, by particle emission. These secondary particles will carry off most of the excitation energy, neutron emission being favored over charged particle emission because of the Coulomb barrier of the nucleus. The energy distribution will be, roughly, a decaying exponential, with substantially no particles carrying more than about 10 Mev. The angular distribution of these particles will be essentially isotropic.

When the incident deuteron has energy less than about 50 Mev, a particular process which we shall call Butler stripping is important. Since in the deuteron the nucleon separation is large and the binding energy low, just one of the incident nucleons may interact with the surface of the target nucleus. If its momentum is proper, it will be bound into the nucleus to form one particular state of a new nuclide, which may then decay to its ground state. The other nucleon, passing by, must conserve energy, parity, and angular momentum. This means that it may carry energy greater than its initial energy by the amount of the binding energy of the captured nucleon. Further, this "secondary" nucleon, instead of carrying just the momentum it had at the time of capture, will, in addition, possess additional angular momentum so that the conservation laws are satisfied. The resulting angular distribution is just a sum over those angular momentum states which are acceptable. Only a few of these are important, since the magnitude of each contribution is roughly inversely proportional to the angular momentum. The

particles, then, are emitted in a pronounced forward direction, but the peak may be displaced from the axis of symmetry.

At higher deuteron energies, the Butler stripping becomes, in the limit, Serber stripping. In this mechanism the collision is "fast", so that the "secondary" particle, the nucleon which passes by, feels no reaction. In terms of the Butler theory, so many angular momenta are accepted that interference between them washes out the effect. The secondary's final momentum is the result of the motion of the deuteron center of mass, and its motion with respect to the center of mass at the moment the other nucleon is stripped off by the edge of the nucleus. The resulting angular distribution is sharply forward, maximum in the direction of the axis of symmetry, with a half-width of about $3\sqrt{\epsilon_d/T_d}$. The distribution of energies is centered around half the incident deuteron energy, and has a half-width of about $2\sqrt{T_d \epsilon_d}$ where ϵ_d is the deuteron binding energy, and T_d is the incident deuteron kinetic energy. The cross section for this process is proportional to the target nuclear radius.

Another effect which may occur is the "field stripping" described by Dancoff. It is the action of the Coulomb field of the target nucleus upon the incident deuteron. When the energy is low, this amounts to an orientation of the deuteron (because of Coulomb repulsion on the proton), which accounts in part for the high cross section for deuteron reactions. When the energy is sufficiently high, the transverse electric field seen by the moving deuteron may cause it to split up. The angular distribution

from this process is narrower than that of the Serber stripping, by a factor of two, but the total effect is predicted to be as important for heavy elements, since the cross section goes like the square of the charge on the target nucleus.

When the incident nucleon energy is as high as 90 Mev, the nucleus becomes somewhat transparent, because the nucleon-nucleon cross section decreases with energy. This makes the mean free path for nucleons in nuclear matter the order of the radius of the nucleus, so that if a collision occurs, one or more fast secondary particles may be emitted. The angular and energy distributions of the "knock-on" secondaries will depend upon the model chosen for the nucleus, but at least partial correlation is expected with the direction and energy of the incident nucleons, so that the secondaries will be emitted mainly forward, with energies equal to that of the incident nucleons, or less.

Chew and Goldberger have described a process by which deuterons, tritons, etc. may be produced. The nucleons within the nucleus are in motion, and when an incident nucleon penetrates, there is some probability that a pair may result in such a momentum relationship that, say, a deuteron is formed. If the total energy is high, so that the mean free path is long, this "pick-up" deuteron may escape as a secondary. Three-particle pick-up will result in a triton or He^3 secondary. These "pick-up" particles will be emitted strongly forward, and they will be peaked around some energy which gives the best compromise between the formation probability, which involves the internal nucleon momentum distribution, and the escape probability.

High energy fission can also occur when heavy nuclei are bombarded by nucleons. The secondary nucleons, mainly neutrons are emitted isotropically and with energy less than 10 Mev.

The features described above are collected in the following table.

NAME OF PROCESS	BOHR COMPOUND NUCLEUS	BOHR AND WHEELER FISSION	BUTLER STRIPPING	SERBER STRIPPING	DANCOFF FIELD STRIPPING	GOLDBERGER KNOCK-ON'S	CHEW AND GOLDBERGER PICK-UP
DESCRIPTION OF PROCESS	Incident nucleon shares energy quickly to form excited compound nucleus; secondaries are evaporated	Incident nucleon excites heavy nucleus, which boils, splits in two, with secondaries emitted	Incident nucleon is captured in a resonance process. secondary conserves energy, parity, and momentum	Incident nucleon stripped off and ignored; secondary unaffected by collision	Incident proton sees transverse electric field and splits off; secondary affected	Incident nucleon makes a "knock-on" secondary by collision with a nucleon in the nucleus	Incident nucleon "picks up" target nucleons, if momentum right for creation and escape
IMPORTANT WHEN INCIDENT DEUTERON ENERGY, T_d, IS	$T_d < 90$ Mev	$T_d < 90$ Mev	$T_d < 50$ Mev	$T_d > 50$ Mev	$T_d > 50$ Mev	$T_d > 150$ Mev	$T_d > 150$ Mev
APPEARANCE OF TARGET NUCLEUS TO INCIDENT NUCLEONS	Opaque; short mean free path	Opaque; short mean free path	Opaque; short mean free path if incident energy is "proper"	Either opaque or transparent; incident nucleon ignored	Point source coulomb field	Transparent; mean free path of order of nuclear radius	Transparent; mean free path of order of nuclear radius
KINDS OF SECONDARIES	Mainly neutrons, some protons	Neutrons	Neutrons and protons equally	Neutron and protons equally	Neutrons and protons equally	Neutrons, protons	Mainly deuterons, some tritons, He^3's
ANGULAR DISTRIBUTION OF SECONDARIES (ALL ENERGIES)	Essentially isotropic	Isotropic	Sharp forward peak, which is off symmetry axis, in general	Sharp forward peak on axis of symmetry	Sharp forward peak off axis of symmetry	Broad forward peak; position depends on nuclear model	Sharp forward peak on axis of symmetry
ENERGY DISTRIBUTION OF SECONDARIES (ALL ANGLES)	$T_s < 10$ Mev Maxwellian $(T_s)_{max} \approx 2$ Mev	$T_s < 10$ Mev Maxwellian $(T_s)_{max} \approx 1$ Mev	T_s sharply peaked around $T_d/2$ + binding energy of captured nucleon	T_s sharply peaked around $T_d/2$	T_s sharply peaked around $T_d/2$	$T_s < T_d/2$ decrease with energy	$T_s < T_d/2$ peaked around "proper energy"

The aim of the present work was an investigation of the high energy charged secondary particles (proton energy > 26 Mev, deuteron energy > 35 Mev) from bombardment of beryllium, carbon, and uranium nuclei by 190 Mev deuterons. The information to be gained includes (a) the relative importance of the deuteron's binding energy in collisions with nuclei, (b) a measurement of the cross section for stripping, and (c) evidence for the existence of Dancoff field stripping.

III EXPERIMENTAL METHOD

A. Some General Remarks on Differential Scattering Cross Sections

A differential scattering cross section is sometimes defined by a certain equation, the equation usually being of the sort

$$C = nN_t\Omega\frac{d\sigma}{d\Omega}(\Phi) \qquad (1)$$

where C = number of counts observed in the detector

n = number of particles incident upon the target

N_t = number of target nuclei per cm^2 in the beam

Φ = angle between beam direction and the detector

Ω = solid angle subtended by the detector at the target.

A cross section of this kind is of a very special nature, and it is of interest to investigate the problem more generally, to determine the approximations which are implicit in the usual definitions.

Consider an inelastic scattering process, defined to be one in which the particles emitted at a given mean angle Φ_o include a more or less broad spectrum of energies. In such a case, the connection between the observation and the differential scattering cross section is given by

$$C(\Phi_o,T_o,T_o') = \iiint J(T')N\frac{d^2\sigma}{d\Omega dT}(\Phi,T,T')P(T,\Omega)d\Omega dTdT' \qquad (2)$$

$C(\Phi_o,T_o,T_o')$ = number of counts observed in the detector when it is set to accept particles of mean energy T_o at mean angle Φ_o, when particles of mean energy T_o' are bombarding the target.

$J(T')$ = number of incident particles whose energies lie between T' and $T' + dT'$. The integration is over all T'. $\int J(T')dT' = I$ = total number of particles incident upon the target. The beam particles are assumed to be independent of each other.

N = number of target nuclei per cm^2 in the beam direction, and is assumed to be constant.

$\frac{d^2\sigma}{d\Omega dT}(\Phi, T, T')$ = differential scattering cross section in the laboratory system for producing particles of energy T at angle Φ when the target nucleons are bombarded with particles of energy T'.

$P(T, \Omega)$ = detector resolution probability function which describes how efficiently a particle of energy T emitted into a solid angle Ω will be detected.

Thus the observation is an aggregate measure of events which result from bombardment over a range of energies T', on a target which emits particles over a range of energies T, and angles Φ, and which the detector system accepts over some energy interval ΔT, about T_o, within a band of angles $\Delta\Phi$ about Φ_o. T_o, T_o' and Φ_o are the nominal values ascribed to the system.

Let us now consider the use of such an equation in analyzing an experiment. It is of course desirable to use a beam of monoenergetic

particles on the target. By monoenergetic is meant a spread in energies which is small compared to the nominal beam energy. Such a beam is available, for example, from the linear accelerator, from the 345 Mev proton beam, and from the 190 Mev deuteron beam. In such a case, it is a good approximation to put

$$\int J(T')dT' = I(T_o')$$

so that

$$C(\Phi_o, T_o, T_o') = I(T_o')N \iint \frac{d^2\sigma}{d\Omega\, dT}(\Phi, T, T_o')P(T, \Omega)d\Omega\, dT \qquad (3)$$

The assumption here is that the differential scattering cross section is constant over the range of T' around T_o' in the incident beam. When the 90 Mev neutron beam is used, with its 30 Mev width, the approximation becomes correspondingly worse, and the meaning of the "measured" differential cross section is not so clear.

The next step in an experiment is to make the spread in energies and angles accepted by the detector as small as is feasible. Then, if the detector resolution is good, we can write

$$C(\Phi_o, T_o, T_o') = I(T_o')N \frac{d^2\sigma}{d\Omega\, dT}(\Phi_o, T_o, T_o') \iint P(T, \Omega)d\Omega\, dT \qquad (4)$$

which assumes that $d^2\sigma/d\Omega dT$ is only slowly varying over the small range of Ω and T which the counter accepts.

The integral

$$\iint P(T, \Omega)d\Omega\, dT = \Delta\Omega_o \Delta T(T_o) \qquad (5)$$

must now be evaluated from an analysis of the detector resolution. It

should be emphasized that the ΔT of the integral is not, in general, the range of energies accepted by the detector, which is what is represented on a histogram, but is a quantity which must be determined by a careful consideration of the type of detector used.

When this is done, our equation becomes

$$C(\Phi_o, T_o, T_o') = I(T_o')N \frac{d^2\sigma}{d\Omega dT}(\Phi_o, T_o, T_o')\, \Delta\Omega_o \Delta T(T_o) \qquad (6)$$

from which

$$\frac{d^2\sigma}{d\Omega dT}(\Phi_o, T_o, T_o') = \frac{C(\Phi_o, T_o, T_o')}{\Delta\Omega_o I(T_o')N\, \Delta T(T_o)} \qquad (7)$$

An example of the use of such a cross section is the d-p reaction.

In the case of elastic processes, it has no meaning to write the differential scattering cross section as above. Since the angle, and energy are uniquely related, the dependence of the cross section and of the resolution function includes only one of them, usually the angle. Thus we write

$$C(\Phi_o, T_o') = \iint J(T')N \frac{d\sigma}{d\Omega}(\Phi, T')P(\Phi)dT'd\Omega \qquad (8)$$

and, again, under proper conditions,

$$C(\Phi_o, T_o') = I(T_o')N \frac{d\sigma}{d\Omega}(\Phi_o, T_o') \int P(\Phi)d\Omega \qquad (9)$$

By an analysis of the detector resolution, we can evaluate

$$\int P(\Phi)d\Omega = \Delta\Omega(\Phi_o)$$

so that

$$C(\Phi_o,T_o) = I(T_o')N \frac{d\sigma}{d\Omega}(\Phi_o,T_o')\Delta\Omega(\Phi_o) \qquad (10)$$

Equations of type (10) were used in (n,p) and (p,p) scattering experiments. It must be emphasized again that $\Delta\Omega(\Phi_o)$ in general is not the solid angle subtended by the detector slit, although in particular detection systems it may be. Equation (1) is an example of a special case of (10).

If an experiment is done on light elements, it is possible that an inelastic scattering from one isolated level of known energy can be examined. In such a case, the differential scattering cross section as defined in (8) is valid, with the energy balance adjusted from the known level height.

For the purposes of the present experiment, which involves inelastic cross sections only, it was sufficient to detect charged particles, without trying to discriminate between them. It was already known that the secondary particles would be mainly protons, with some deuterons, and the numbers of other kinds of charged particles would be negligibly small, due to the small cross section for their production. Equation (2), generalized, becomes, in such a case,

$$C(\Phi_o,T_o^j,T_o') = \sum_j \iiint J(T')N \frac{d^2\sigma^j}{d\Omega\, dT^j}(\Phi,T^j,T')P(T^j,\Omega)d\Omega\, dT^j dT' \qquad (11)$$

where the sum is over the j different kinds of secondaries. $\frac{d^2\sigma^j}{d\Omega\, dT^j}$, is the differential cross section for producing a type j secondary

particle of energy T^j, at angle Φ, when the incident energy is T'. Under suitable approximations, as explained

$$C(\Phi_o,T_o^j,T_o') = I(T_o')N \sum_j \frac{d^2\sigma^j}{d\Omega dT^j}(\Phi_o,T_o^j, T_o')\iint P(T^j,\Omega)d\Omega dT^j \qquad (12)$$

The relation between angle and energy for the emitted particles is not explicitly known in inelastic scattering, so the resolution function P must be written in terms of both angle and energy. Let us assume that it can be written

$$P(T,\Omega) = P(T)\pi(\Omega) \qquad (13)$$

Let us further assume that if the particle is emitted into the solid angle $\Delta\Omega_o$, subtended by the slit, it will certainly be counted, and if it is emitted outside this $\Delta\Omega_o$, it will certainly not be counted. Then

$$\pi(\Omega) = 1 \qquad \text{over all } \Delta\Omega_o \qquad (14)$$

and

$$\int \pi(\Omega)d\Omega = \Delta\Omega_o \qquad (15)$$

Equation (12) then becomes

$$C(\Phi_o,T_o^j,T_o') = I(T_o')N\Delta\Omega_o \sum_j \frac{d^2\sigma^j}{d\Omega dT^j}(\Phi_o,T_o^j,T_o')\int P(T^j)dT^j \qquad (16)$$

In order to evaluate the integral, an analysis of the detector energy resolution must be made.

B. Detector Energy Resolution

In the present investigation, the emitted charged particles were detected by a differential-range measuring device. These charged secondaries, in order to be counted were required to traverse the first three chambers of a proportional counter telescope, (in coincidence) and stop in a thin range foil before reaching the fourth chamber (anti-coincidence). (See Figure 1.) The secondary particle energies are measured by varying the thicknesses of aluminum absorbing foils placed in front of the counter telescope, and applying the range-energy relationship.

Consider a specific proton which has been produced by a (d,p) reaction exactly at the midpoint of the target. Suppose this proton, moving at an angle Φ_o (in the laboratory system) to the original beam direction, has energy just sufficient to carry it through

(a) the remaining target thickness

(b) the air path between the target and the counter telescope

(c) the aluminum absorber

(d) the first three chambers of the telescope, and

(e) exactly half the range-foil thickness.

Such a path defines a specific proton energy T_o. However, both the converter and the range-foil have finite thicknesses, and even monoenergetic particles straggle in range. This means that the

detection system has a finite energy resolution; when it is set to detect protons of energy T_o, it accepts protons whose energies lie within a band around T_o. In general, the detector will not accept all protons within the band with equal efficiency. Rather, the resolution of the system is some function of those effects mentioned above, and will, in addition, depend strongly upon T_o. If each of the individual effects can be represented analytically, the resolution of the system will be defined by the "fold" of the analytical functions which describe these effects.

One example of such a fold function is

$$F(t) = \int_{-\infty}^{\infty} f(x)g(t - x)dx. \tag{17}$$

For this problem, we will assume that the final resolution of the detector is given by

$$P(T) = \int_{-\infty}^{\infty} p_c(T - E) \int_{-\infty}^{\infty} p_b(K)p_a(E - K)dKdE \tag{18}$$

where $p_a(T)$ = function which describes effect of finite target thickness

$p_b(T)$ = function which describes effect of finite range-foil thickness

$p_c(T)$ = function which describes effect of range straggling.

1. Target. Consider the effect of the finite target thickness. We wish to determine the probability $P(T)dT$ that a proton,

produced at a point t in the target, at an angle Φ_o exactly, and with an energy just sufficient (with no straggling) to reach the midpoint of the range-foil, has an energy between T and T + dT. Since the energy and the range are uniquely related, we can write

$$p(t)dt = p_a(T)dT$$

where p(t) is the probability that the proton was produced between t and t + dt in the target. We will assume this to be a constant, since the target is thin, and the incident beam sees all the target nucleons along its path.

$$p(t) = \text{constant} = K_1$$

also, since

$$R \cong k' T^{1.8}$$

$$dt = dR = k_2 T^{0.8}$$

so that

$$p_a(T) = K_1 K_2 T^{0.8}$$

or, lumping constants together,

$$p_a(T) = k_a T^{0.8} \quad \text{between } T_{max} \text{ and } T_{min}.$$

Since the particle from the target certainly has <u>some</u> energy,

$$\int_{-\infty}^{\infty} p_a(T)dT = 1$$

so that

$$k_a = \frac{1.8}{T_{max}^{1.8} - T_{min}^{1.8}}$$

The limits of the energy width T_{min} and T_{max} are determined by a consideration of the total thickness, L, of the target.

A proton which is made at the midpoint of the target has energy T_o. If it is made at the front, or beam side of the target, it will have energy

$$T_{max} \cong T_o + \left(\frac{dT}{dx}\right)_{T_o} x \frac{L}{2}$$

and if made at the back, or counter side of the target, it will have energy

$$T_{min} \cong T_o - \left(\frac{dT}{dx}\right)_{T_o} x \frac{L}{2}$$

2. Range-Foil. Consider the effect of the range-foil upon the energy resolution. If the particle has a range between R_{min} and R_{max}, the limits of the range-foil, it will certainly be counted. In fact, all particles with range between these limits will be counted with unit probability. Since to every range there corresponds a unique energy (neglecting straggling), the energy limits of the range-foil are T_{min} and T_{max}.

Hence

$$p_b = 1 \text{ between } T_{min} \text{ and } T_{max}$$

and

$$\int_{-\infty}^{\infty} p_b(T)dT = \Delta T.$$

If the range-foil is ΔR mg/cm^2 thick,

$$T_{min} \cong T_o - \left(\frac{dT}{dx}\right)_{T_o} \times \frac{\Delta R}{2} ,$$

$$T_{max} \cong T_o + \left(\frac{dT}{dx}\right)_{T_o} \times \frac{\Delta R}{2} ,$$

and

$$\Delta T(T_o) = T_{max} - T_{min} \cong \left(\frac{dT}{dx}\right)_{T_o} \cdot \Delta R$$

If the proton had stopped, not in the range-foil but in the front half of the third chamber, and had given a sufficiently high pulse to be counted, or in the front half of the fourth chamber, and had not given a sufficiently high pulse to be counted, there would be an uncertainty of about 3 mg/cm^2 of aluminum equivalent in determining where the particle had actually stopped. Since the range-foil is 760 mg/cm^2 of aluminum equivalent, this uncertainty in range is ~0.4 percent.

3. Straggling. Consider the effect of range straggling of the protons. We wish to determine the probability $p_c(T)dT$ that a proton, produced at the midpoint of the target, at an angle Φ_o exactly, and then stopping at the midpoint of the range-foil, has an energy between T and T + dT. Since every energy produces some range, we can write

$$p(R)dR = p_c(T)dT$$

where $p(R)dR$ is the probability that a particle of energy T_o will have a range between R and R + dR. From straggling theory, this is the

Gaussian

$$p(R) = Ae^{-\frac{(R - R_o)^2}{2(\Delta R)^2}}$$

and we approximate

$$p_c(T) = k_c e^{-\frac{(T - T_o)^2}{2(\Delta T)^2}}$$

Since the particle certainly has some range,

$$\int_{-\infty}^{\infty} p_c(T)dT = 1$$

so that $K_c = \frac{1}{\Delta T \sqrt{2\pi}}$

From straggling theory, we get

T_o	20	50	65	100	120	150
$(\Delta T)_{Mev}$	0.25	0.5	0.65	1.05	1.25	1.5

C. The Integral of the Resolution Function

Since we have assumed that the form of the fold of two functions is given by

$$F(t) = \int_{-\infty}^{\infty} f(x)g(t - x)dx \qquad (17)$$

the area under the resulting fold is just

$$\int_{-\infty}^{\infty} F(t)dt = \int_{-\infty}^{\infty} \int_{-\infty}^{\infty} f(x)g(t - x)dxdt \qquad (19)$$

Reversing the order of integration

$$\int_{-\infty}^{\infty} F(t)dt = \int_{-\infty}^{\infty} f(x)dx \int_{-\infty}^{\infty} g(Z)dZ \qquad \text{where } Z = t - x \qquad (20)$$

That is, the area under the resulting fold is equal to the product of the areas of the functions which are being folded.

Now, as we have shown,

$$\int_{-\infty}^{\infty} p_a(T)dT = 1$$

$$\int_{-\infty}^{\infty} p_b(T)dT = (\Delta T)_{T_o}$$

$$\int_{-\infty}^{\infty} p_c(T)dT = 1$$

Hence

$$\int_{-\infty}^{\infty} P(T)dT = \int_{-\infty}^{\infty} p_a(T)dT \int_{-\infty}^{\infty} p_b(T)dT \int_{-\infty}^{\infty} p_c(T)dT = \Delta T(T_o) \qquad (21)$$

where

$$\Delta T(T_o) \cong \left(\frac{dT}{dx}\right)_{T_o} \cdot \Delta R$$

is the energy bite taken by the range-foil when the mean proton energy is T_o.

An example of the fold is shown in Figure 2 for a mean proton energy $T_o \approx 155.7$ Mev. The fold was done graphically. While the detector resolution is 4 Mev wide at half-maximum, the integral of the resolution function is a bite in energy only about 1.5 Mev wide. The fold also indicated that the best resolution for a given counting intensity was to be obtained by making the range-foil and target of equal range.

Equation (16) can now be written

$$C(\Phi_o, T_o^j, T_o') = I(T_o')N\Delta\Omega_o \sum_j \frac{d^2\sigma^j}{d\Omega dT^j}(\Phi_o, T_o^j, T_o')\Delta T(T_o^j) \qquad (22)$$

The analysis of the resolution and its integral for secondary deuterons is similar to that for protons.

The value of the integral of the detector resolution function is shown in Figure 3 for both protons and deuterons. If equation (22) is correct, it should be possible to vary each of the parameters independently, and test the linear dependence of the counting rate on each.

D. Observable Secondary Particles

The lower limit to the energies of the secondary particles which can be detected is set by the minimum range which each particle must have in order to just reach the range-foil in the detector. This minimum energy is 26 Mev for protons, and 35 Mev for deuterons.

Regarding the incident deuteron as two essentially independent nucleons, the processes which will be observed in this experiment are the result of the incident proton interactions with the nucleus to yield (a) knock-on protons or (b) pick-up deuterons, and the incident neutron interactions with the nucleus to yield (a) stripped protons, (b) knock-on protons and (c) pick-up deuterons. While the incident neutron interacts only with sub-nuclear protons to yield an observable particle (protons of energy > 26 Mev, deuterons of energy > 35 Mev), the incident proton can interact with either neutrons or protons. The counts

observed when the detector is set at some mean angle Φ_o, and for particles of mean energy T_o^j, will be

$$C_{Total} = C_1(d,p) + C_2(n,p) + C_3(p,p) + C_4(p,n) + C_5(p,d) + C_6(n,d).$$

In terms of cross sections, equation (17) is just

$$C = IN\Delta\Omega_o\left\{\Sigma_p\Delta T_p + \Sigma_d\Delta T_d\right\} \tag{23}$$

where

$$\Sigma_p = \frac{1}{A}\left\{(A-Z)\ \frac{d^2\sigma(p,n)}{d\Omega\,dT} + Z\,\frac{d^2\sigma(p,p)}{d\Omega\,dT} + Z\,\frac{d^2\sigma(n,p)}{d\Omega\,dT}\right\} + \frac{d^2\sigma(d,p)}{d\Omega\,dT}$$

$$\Sigma_d = \frac{1}{A}\left\{(A-Z)\ \frac{d^2\sigma(p,d)}{d\Omega\,dT} + Z\,\frac{d^2\sigma(n,d)}{d\Omega\,dT}\right\}$$

ΔT_p = energy bite taken by range-foil for protons

ΔT_d = energy bite taken by range-foil for deuterons.

IV THE DIFFERENTIAL-RANGE COUNTER TELESCOPE CHARACTERISTICS

A convenient method of determining the energy of a charged particle is to measure its range in matter. A simple scheme for range determination is to set up two counters, placing between them some material in which the incident charged particle will lose energy by the ionization of the atoms of the material. Then, the number of particles which have stopped in the range-foil is the number which have passed through the first counter, minus the number which have passed through both counters in coincidence. In order to reduce the number of accidental coincidences due to background from the cyclotron, and to define more sharply the direction from which the particles come, a four-chamber proportional counter telescope was used in this experiment. The number of particles which have stopped in the range-foil is then the number which traverse the first three chambers in coincidence, minus the number which traverse all four chambers in coincidence.

This method of counting, however, introduces spurious counts which are the result of (a) imperfect counting of particles in the fourth chamber, and (b) nuclear attenuation of particles in the range-foil.

The number of triple coincidences which register in the first three chambers of the telescope is

$$\gamma = \int_{T_{min}}^{\infty} \eta_{123}(T) F(T) dT \qquad (24)$$

where

η_{123} = combined total efficiency of the first three chambers for counting charged particles

$F(T)$ = energy spectrum of charged particles which can enter the counter

T_{min} = energy which a particle must have in order just to reach the front face of the range-foil; that is, the back of the third chamber.

γ consists of the two terms

$$\gamma = \int_{T_{min}}^{T_{max}} \eta_{123} F(T)dT + \int_{T_{max}}^{\infty} \eta_{123} F(T)dT \qquad (25)$$

where T_{max} = energy which a particle must have in order just to reach the back face of the range-foil; that is, the front of the fourth chamber. The first term of (25) includes just the desired counts; those particles which actually end their range in the range-foil. The second term of (25) accounts for those particles which have energy great enough to carry them into the fourth chamber or beyond. If the counter is to accept only the desired counts, the fourth chamber must detect all of the contributions from the second term. Of the latter, only

$$Q = \int_{T_{max}}^{\infty} \eta_{123} \eta_4 F(T)dT \qquad (26)$$

will register as quadruple coincidences. η_4 is the efficiency of the

fourth chamber, and is less than unit because

(a) particles which have energy sufficient to enter the fourth chamber may have been scattered enough to be missed.

(b) The energy loss in the fourth chamber, being statistical, may fluctuate enough so that some particles are not counted.

(c) The pulse from the fourth chamber may be delayed sufficiently (longer electron collection time in the counter, or electronic circuit delays) for some particles to be missed.

If η_4 is indeed less than unity, then spurious counts will be included in the second term of the observed quantity

$$\gamma - Q = \int_{T_{min}}^{T_{max}} \eta_{123} F(T)dT + \int_{T_{max}}^{\infty} \eta_{123}(1 - \eta_4)F(T)dT \qquad (27)$$

Ideally, the counter-telescope should be operated so that the first three chambers are sensitive only to charged particles which will stop in the range-foil. Then there would be no quadruple coincidences and no spurious contribution. In practice, such operation is impossible, since range straggling, fluctuations in pulse heights, and jitter require rather high efficiencies on the first three chambers. From equation (27) it can be seen that the spurious counts can be minimized by making η_4

as large as possible, and η_{123} as small as possible for particles of energy $> T_{max}$. η_4 can be made large by

(a) making the fourth chamber large enough in extent so that few particles are scattered enough to be missed;

(b) making the fourth chamber deep, so that the effect of statistical fluctuations are minimized. The discriminator bias should be set low, and the amplifier gain set high on the fourth electronics channel for the same reason. The fourth chamber might well be a scintillator, viewed by one or more photomultipliers. This type of counter can be very efficient as the last chamber of a telescope since it can then be made thick enough to stop all the particles.

(c) gating the fourth channel "on" sufficiently long so that both counter and electronics jitter do not cause counts to be missed.

η_{123} can be made small for particles of energy greater than T_{max} by raising the discriminator bias on the first three channels to a point where most of the particles whose original energy was greater than T_{max} are not counted, but all the desired particles with energy $T_{min} < T < T_{max}$ are still accepted. This is possible since these latter particles are losing energy at a greater rate than the former, so that their pulse heights in the first three chambers are greater.

Still another complication arises from the fact that some of those particles, which should register as quadruples, will be removed by nuclear encounters in the range-foil. Of Q such particles incident on the range-foil, only $Qe^{-\sigma t}$ will be left to fire the fourth chamber after traversing t nucleons per cm^2 of range-foil. The total nuclear attenuation cross section, σ, can be approximated by an average value over the energies which the particles, whose initial energies lay between $T_{max} < T < \infty$ actually have while traversing the range-foil.

The observed counts thus consist of the two terms

$$\delta = \gamma - Q = \int_{T_{min}}^{T_{max}} \eta_{123} F(T)dT + \int_{T_{max}}^{\infty} \eta_{123}(1 - \eta_4 e^{-\sigma t})F(T)dT \qquad (28)$$

In general, t can be kept small compared to the total range, and σ is also small, so that we can expand the exponential, giving

$$\delta = \delta_o + \int_{T_{max}}^{\infty} \eta_{123}(1 - \eta_4)F(T)dT + \int_{T_{max}}^{\infty} \eta_{123}\eta_4 \sigma t F(T)dT \qquad (29)$$

to first order, where $\delta_o = \int_{T_{min}}^{T_{max}} \eta_{123} F(T)dT$ are the desired events.

Actually, the efficiencies are functions of the particle energies, since the ionization loss in each chamber is a function of the energy. For simplicity, we can define an average efficiency for the fourth chamber,

$$\bar{\eta}_4 = \frac{\int_{T_{max}}^{\infty} \eta_4 F(T)dT}{\int_{T_{max}}^{\infty} F(T)dT} \qquad (30)$$

η_4 is no longer dependent on the energy, but is now, through T_{max}, a function of that portion of the spectrum being investigated. Dropping the average signs, (29) can now be written

$$\delta = \delta_o + (1 - \eta_4)\int_{T_{max}}^{\infty} \eta_{123} F(T)dT + \sigma t \eta_4 \int_{T_{max}}^{\infty} \eta_{123} F(T)dT \qquad (31)$$

Now the desired counts, given by δ_o, are proportional to the thickness of the range-foil, in mg per cm^2

$$\delta_o = K_1 R$$

and the thickness t, in nucleons per cm^2, can be expressed in terms of R in mg per cm^2

$$t = \frac{L_o}{A} R$$

where A = atomic weight

L_o = Loschmidt's number

so that

$$\delta = (K_1 + \sigma \eta_4 \frac{L_o}{A} Y)R + (1 - \eta_4)Y \qquad (32)$$

where $$Y = \int_{T_{max}}^{\infty} \eta_{123} F(T)dT \qquad (33)$$

From equation (32), it can be seen that the observed quantity, δ, is proportional to the thickness R of the range-foil. In order to reduce the spurious counts, it is advantageous to use a material for the range-foil which has the smallest attenuation cross section for the largest

stopping power. For a given R, the stopping power is approximately proportional to Z/A, while σ is approximately proportional to $A^{2/3}$. Thus, we wish to maximize

$$\frac{\frac{dE}{dx}}{\frac{\sigma}{A}} \propto \frac{\frac{Z}{A}}{A^{-1/3}} = \frac{Z}{A^{2/3}}$$

Material	$Z/A^{2/3}$
Al	1.44
Cu	1.84
Ta	2.25
U	2.40

From the above table it is clear that a high A material should be used for the range-foil.

While it is true that the scattering in a high Z material will be increased, it is not considered in this problem, since it is presumed that the fourth chamber will be made sufficiently large in lateral dimensions to detect the scattered particles. This will be the case in the present experiment, since, when the detector is set to detect low energy particles, many high energy particles will still traverse the telescope with only small scattering. For other applications, it may be important to minimize the scattering rather than the nuclear attenuation, in which case a low Z material should be used.

V APPLICATION OF EXPERIMENTAL METHOD

A. General Procedure

The experimental arrangement is shown in Figure 4. The collimated external deuteron beam of the 184-inch cyclotron was monitored by an argon-filled ionization chamber whose collected charge was integrated electronically. The targets were thin and larger in lateral extent than the beam. They were placed in the beam and the emitted charged secondary particles were detected by a proportional counter telescope. This detector was shielded with lead from any particles which might have scattered either from the mouth of the collimator or from the ionization chamber. The number of incident deuterons was determined from the charge collected in the ionization chamber, and the number of secondaries produced at mean angle Φ_0 into the solid angle defined by the slit was determined from the counts in the telescope. The range of each particle measured its energy. The effects of the air path of the incident beam and the general cyclotron background were removed by using no target on alternate runs. The target-blank difference thus measured the intensity of secondary particles which came from the target.

B. Beam and Alignment

The source of deuterons for the experiment was the full energy circulating beam from the 184-inch synchrocyclotron. These deuterons were multiply scattered[7] into the magnetic deflector channel, and steered into a shielded enclosure where the experiment was carried out (Figure 5). The beam pulse obtained this way is of about 40 microseconds duration, with a repetition rate of about 60 pulses per second.

The deuteron energy is fixed by the path through the magnetic deflector channel and the steering magnet. This energy was determined from the curvature in the magnetic field, and from the range in aluminum, and corresponds to approximately 190 Mev. The variation in energy is thought to be less than $\pm$ 2 percent.

The beam was collimated by means of a four foot brass plug so that it was about 1/2 inch in diameter when it emerged from the shielding. The position and spread of this beam were measured by the blackening produced on x-ray films placed at several points along the beam path. The surface of the table which supported the apparatus was then oriented parallel to the plane containing the beam, target, and detector. The table was also adjusted so that fiducial marks inscribed for the purpose fell along the beam path as defined by the films. The alignment was checked frequently by means of films to insure that it was correct at each angular setting of the detector. The alignment is thought to be accurate to $\pm$ 1/2 degree.

In order to insure that the counts varied linearly with the number of deuterons incident, as indicated by equation (16), the beam intensity was adjusted so that the coincidence counting rate $\gamma - Q$ per unit of collected charge was constant as a function of beam intensity. The beam intensity was always chosen so that the singles rate in any one chamber was about one count per beam pulse, since at this counting rate the number of accidental γ coincidences is negligible, as was shown by the beam plateau.

C. Beam Monitor

The deuteron beam was monitored with an argon-filled ionization chamber, whose multiplication factor for 190 Mev deuterons as determined by comparison with a Faraday cup, was 1525 charges collected per deuteron. The charge collected by the ionization chamber was placed on a low-leakage condenser connected to the input grid of an integrating electrometer (Figure 6). The electrometer was of the 100 percent feedback type, and drove a continuous recorder which recycled itself after reaching a predetermined voltage. The recording circuit automatically calibrated itself periodically against a standard cell.

The condenser used was calibrated by means of an impedance bridge against a standard condenser whose capacitance is known to about 0.1 percent. The monitor system is believed to be accurate to $\pm$ 2 percent.

D. Targets

The beryllium, carbon, and uranium foil targets used in the experiment were all thin ($\sim$ 700 mg per cm^2) and cut from stock materials. These foils were mounted on a carriage which could be driven from a remote position. This arrangement made it simple to change targets with a minimum loss of running time, and a single no-target run sufficed to determine the background subtracted from all three targets for any one angle and energy determination. The targets were about 2 inches square, larger in lateral dimensions than the beam. This was checked photographically for the minimum and maximum angular

positions of the target. The target carriage rotated upon a mount which also contained the detector telescope, and the target surface was at all times perpendicular to the line joining the target and the detector. The target thicknesses were made as nearly equal as possible, so that a change of target had a negligible effect upon the resolving power of the apparatus.

E. Absorber Correction

At the deuteron energy used in this experiment, the absorbers used to measure the emitted particle energies are so thick (up to several gm/cm^2) that some particles which would otherwise pass through are removed by Rutherford scattering and nuclear absorption. The fraction of particles lost in this way is proportional to

$$N\left[\sigma_R(T) + \sigma_A(T)\right]$$

where N is the number of atoms per cm^2 in the absorber, σ_R is the Rutherford cross section of the absorber for scattering protons through an angle so great that they would not be counted, and σ_A is the cross section for nuclear absorption in aluminum. Rather than calculate these effects for a variety of energies, an experiment was performed to determine them. The experiment consisted in making an integral range determination with protons. A Faraday cup was used to collect protons which came from the cyclotron after they had passed through an ionization chamber and an absorber of thickness t. The relative yield was then plotted as a function of absorber thickness and this

served as a correction factor, normalized to unity at zero absorber thickness. The maximum correction factor used was of the order of 25 percent. The correction curve for protons is shown in Figure 7. The attenuation cross section for deuterons in aluminum is approximately twice that for protons.[8]

F. Detector

The detector consisted of a four-chamber proportional counter telescope, in front of which was placed a lead slit. The slit, two inches thick, had an opening one inch square which, at a distance of 30 inches from the target, defined the solid angle $\Delta\Omega_0$. In order to test that the counting rate varied linearly with solid angle as predicted by equation (16), a determination of counting rate was made as a function of the reciprocal of the square of the distance between the target and the slit. The dependence is shown in Figure 8 to be linear.

Each chamber of the telescope consisted of a multi-wire, parallel-plate proportional counter, whose dimensions were 3 inches by 3 inches by 1-1/2 inches. The counter wires were made of 0.003 inch nickel, supported under spring tension by teflon bars between brass frames. The spacing between wires was 3/4 inch. The chamber volumes were defined by 0.0005 inch aluminum foils which were fastened across the brass frames. All the components were cleaned with chemicals and then rinsed with water. All four chambers were then mounted into a gas-tight box which was designed in such a way as to allow the range-foil to be inserted between the third and fourth chambers from outside

the box. A thin aluminum window allowed the particles to enter the telescope, and the electrical connections were brought out through kovar seals in the roof of the box. After assembly, the box and its components were outgassed, flushed, and then filled with a mixture of 96 percent argon and 4 percent CO_2 to a pressure of one atmosphere.

The chambers were operated at about 2300 volts and the linear amplifier gains were adjusted so that the largest pulses were not quite overloading. Under these conditions, the typical plateau obtained by plotting the γ-Q coincidence rate against the discriminator bias setting on the first three chambers was adequate (Figure 9).

To test whether the fourth chamber was large enough in lateral dimensions to accept most of the particles from the one inch slit, the γ-Q coincidence rate was determined as a function of the amount of counter area open. This was done by putting a very thick shield in front of the fourth chamber and withdrawing it vertically. Figure 10 shows that the main portion of the particles accepted by the slit lay well within the 3 inch by 3 inch face of the fourth chamber.

To test whether the yield does indeed vary as predicted by Eq. (32), runs were made using protons varying only the range-foil thickness R, and the material of the range-foil. The results are shown in Figure 11. The variation of yield with the range-foil

thickness R is linear, and the slope of the curves does decrease as A increases. Tantalum was chosen as the range-foil material to be used in the experiment, since it was available in foil form in a variety of thicknesses.

Equation (32) also suggests a method by which the magnitudes of the spurious terms can be determined. Since it was known that the yield varies linearly with R, two points on the curve were determined, and the straight line between them was extrapolated back to zero range-foil thickness. When $R = 0$, the only contribution to the yield is from the third term of (32), so the magnitude of this term can be obtained in this way.

This was done for several different settings of the discriminator bias settings on the first three chambers. As this bias increases, Y decreases, since η_{123} decreases. This should affect both the slope of the line, and the size of the residual yield at $R = 0$. The results are shown in Figure 12. As the bias was raised from 20 to 50, no change in slope occurred. A plot of Q over this range shows that Y was indeed changing, so that the conclusion is that the attenuation, represented by the second term of equation (32), was negligible compared to the first term. As the bias was raised above 50, the slope decreases, showing that some of the desired counts were being lost. Thus the investigation showed the proper bias setting which minimized η_{123} without losing the desired counts.

We can now write

$$\delta = \delta_o + Y(1 - \eta_4)$$

and since $Y = \gamma - \delta_o$,

$$\delta = \delta_o + (\gamma - \delta_o)(1 - \eta_4) = \gamma(1 - \eta_4) + \delta_o \eta_4 \qquad (34)$$

or, finally,

$$\delta_o = \frac{\delta - \gamma(1 - \eta_4)}{\eta_4} \qquad (35)$$

Thus, in any given run, δ was observed for two values of R, and the residual $\delta = \gamma(1 - \eta_4)$ at R = 0 determined by extrapolation. η_4 was readily obtainable, since γ was known, so that the desired δ_o could be obtained from equation (35).

G. Electronics

A block diagram of the electronic circuits associated with the operation of the counter telescope is shown in Figure 13. Pulses from the first three chambers generated 2 microsecond gates, and pulses from the fourth chamber generated 3 microsecond gates which overlapped the others in time. The time delay in pulses from the fourth chamber relative to the pulses from the first three chambers was measured by the Q coincidence rate, varying the delay on the gate from the fourth chamber, Figure 14. It is seen that a small but finite contribution was missed, which was a contributing factor

in making η_4 less than unity. This jitter is believed to be the result not only of variation in ion collection time in the counter chambers, but also the effect of the response of the coincidence mixer circuits. The spurious data which resulted was corrected by equation (29).

H. Sample Calculation

As an example, the data taken for $\Phi_o = 15^o$ and $T_o = 26$ Mev on the beryllium target gave

Target	Be	Blank	Be	Blank
Integrated beam (microcoulombs), q	0.4	0.2	0.4	0.2
Range-foil (mils Ta)	21.5	21.5	3.5	3.5
Triple coincidences, γ	16256	599	16096	670
Quadruple coincidences, Q	13040	482	15152	592

The number of particles from the target which apparently stopped in the 21.5 mil range-foil per microcoulomb of incident beam is then

$$(\delta)_{21.5} = \left(\frac{\gamma - Q}{q}\right)_{\text{target in}} - \left(\frac{\gamma - Q}{q}\right)_{\text{target out}}$$

$$= 8040 - 585 = 7455$$

and for the 3.5 mil range-foil,

$$(\delta)_{3.5} = 2360 - 390 = 1970$$

which gives an extrapolated value for the residual spurious background due to the inefficiency of the fourth chamber of

$$\delta_R = 960.$$

From equation (34),

$$\eta_4 \cong 1 - \frac{\delta_R}{\left[\left(\frac{Y}{q}\right)_{\text{target in}} - \left(\frac{Y}{q}\right)_{\text{target out}}\right]_{21.5}}$$

$$\eta_4 = 1 - \frac{960}{\left(\frac{16256}{0.4} - \frac{599}{0.2}\right)} = 0.9745$$

Then, from equation (35) the true counts per microcoulomb are

$$\delta_o = \frac{(\delta)_{21.5} - \left[\left(\frac{Y}{q}\right)_{\text{target in}} - \left(\frac{Y}{q}\right)_{\text{target out}}\right]_{21.5} \times \left[1 - \eta_4\right]}{\eta_4}$$

$$= \frac{7455 - \left(\frac{16256}{0.4} - \frac{599}{0.2}\right)(1 - 0.9475)}{0.9745}$$

$$= 6667$$

Thus, even though the fourth chamber efficiency is ~97.5 percent, the spurious component amounts to about 12 percent, which indicates how important it is to make this correction.

VI RESULTS AND DISCUSSION

A. Presentation of Data

By the method indicated in the sample calculation, the number of particles which stopped in the range-foil per microampere of incident deuteron beam has been determined as a function of energy at laboratory angles of 7.5°, 10°, 15°, 20° and 45°.

A set of composite curves, derived from both theory and experiment, with which to compare these points has been obtained by means of equation (23). The values used for the nucleon-nucleon differential cross sections $\frac{d^2\sigma(n,p)}{d\Omega dT}$, $\frac{d^2\sigma(p,n)}{d\Omega dT}$, and $\frac{d^2\sigma(n,d)}{d\Omega dT}$, were taken from the experiments of Hadley and York,[9] and Hofmann and Strauch.[10] For the uranium target, the results of Hofmann and Strauch were extrapolated from lead. As a first approximation, the differential cross section for producing protons by protons, $\frac{d^2\sigma(p,p)}{d\Omega dT}$, has been taken equal to that for producing protons by neutrons, $\frac{d^2\sigma(n,p)}{d\Omega dT}$, which has been verified in the case of scattering from hydrogen. The differential cross section for deuteron pick-up by protons, $\frac{d^2\sigma(p,d)}{d\Omega dT}$, has been assumed equal to that for neutrons, $\frac{d^2\sigma(n,d)}{d\Omega dT}$. Finally, the shape of the stripping cross section, $\frac{d^2\sigma(d,p)}{d\Omega dT}$, has been computed from the theory of Serber, and normalized to fit the observed points. This theory predicts the differential cross section to be

$$\frac{d^2\sigma(d,p)}{d\Omega dT} = \frac{c\sqrt{T_o}}{\left[\frac{E_d}{2} + T_1 + T_o - 2\sqrt{T_1 T_o}\cos\Phi_o\right]^2} \qquad (36)$$

where T_1 is one-half the incident deuteron kinetic energy, E_d is the deuteron binding energy, Φ_0 is the angle between the beam direction and the emergent nucleon, and T_0 is the kinetic energy of the emergent nucleon.

An example of the construction of a resultant composite yield curve is shown in Figure 15. The variation of the composite curves with angle is shown in Figure 16 for the case of carbon.

Figures 17, 18, and 19 show the data, together with the appropriate composite curves. In these figures, the composite curves have been corrected for absorber attenuation. The data has been normalized to counts per microcoulomb of incident deuterons, and has been corrected for cyclotron background and detector efficiency. The ranges of aluminum used in the experiment have been converted to energies on the proton scale by means of the curves of Aron et al.,[11] for both protons and deuterons which the counter telescope detected, so that a single energy scale suffices for both kinds of particles. The standard deviations shown are due to counting statistics only. The energy resolution of the detector for each point was determined by a graphical integration of equation (18), using the appropriate parameters at each energy.

B. Results

By fitting curves of the shape given by equation (36) to the experimental points at each angle, centered around 90 Mev, values of the proportionality constant c were determined. This enabled the

total cross section for stripping to be computed by integrating equation (36). In view of the fact that stripping has a relatively small dependence upon atomic weight, the beryllium and carbon targets give the same cross sections, within the accuracy of the experiment. For this reason, the cross sections determined from these two elements have been lumped together, and averaged. The results are given in Table I. The weighted averages are

beryllium or carbon	$0.35 \pm 0.03 \times 10^{-24}$ cm^2
uranium	$2.6 \pm 0.4 \times 10^{-24}$ cm^2

The standard deviations were computed from external consistency by assigning a standard deviation to the proportionality constant which was consistent with those attributed to the experimental points. It is felt that this procedure is justified since the constant cannot be varied over wider limits and still have the composite curve fit the data so well.

In addition to the data shown, the charged particle yield was investigated as a function of energy in preliminary experiments at laboratory angles of 90° and 135°. The yields were low, and dropped off rapidly with increasing energy and angle.

C. Conclusions

From the comparison of the experimental points and the composite curves, it can be said that the assumed interactions are indeed the principal collision mechanisms, at least to a first approximation. It is of course to be expected that the deuteron

can be considered as a system of two independent nucleons, since the binding energy (~2.2 Mev) is small compared to the total kinetic energy (~190 Mev).

Beryllium and carbon were chosen as target nuclei in the hope that the loose neutron in beryllium might produce a large effect, compared to a nucleus with a closed structure, like carbon. No such effect was observed.

With respect to the magnitude of the stripping cross section, the values 0.35 barns and 2.6 barns are much larger than the values of 0.12 barn and 0.43 barn which are to be expected from the Serber stripping theory for beryllium and uranium, respectively. Further, this theory predicts an $A^{1/3}$ dependence for the total stripping cross section. However, the values determined in this experiment indicate an $A^{2/3}$ dependence, shown in Figure 20. This discrepancy in magnitude and dependence is not wholly unexpected, in view of the fact that the Serber theory does not include the large contribution to stripping which must result from the transparency of nuclear matter. For example, if the projected deuteron separation is such as to allow both nucleons of the deuteron to fall within the area defined by the nuclear diameter, it would be possible for one nucleon to be removed by collision, while the other passed through the transparent nucleus. For such collisions, the stripping cross section would more closely approximate the geometrical cross section, and a dependence faster than $A^{1/3}$ would result. Of course, the nucleus is not perfectly

transparent, and the diameters of the heavy nuclei are of the order of several mean free paths for the nucleons with which we are concerned. This means that the shape of the differential cross section which was used to fit the data is certainly not correct. However, the shape cannot differ too much from the form used, and still permit a good fit to the data. The accuracy of the experiment does not permit a more detailed description of this enlarged differential stripping cross section.

The large cross section for uranium can be used to explain qualitatively the results of Helmholz et al.[12] in observing the angular distribution of neutrons from deuterons bombarding uranium targets. Their angular distribution fitted the shape predicted by the Serber theory alone. Now the Dancoff cross section for electric field stripping was predicted to be about 0.1 barn in uransium, compared to 0.43 barn for the Serber process. Therefore, since the angular distribution from electric stripping is much narrower than that from the Serber theory, a total angular distribution is to be expected that is somewhat narrower than was observed, corresponding to a superposition of these two effects. This was hard to understand, as long as the Serber process was the only expected one. However, comparing the 0.1 barn for electric stripping in uranium to the enlarged stripping cross section of 2.6 barns, with its angular distrition similar to that of Serber, the results of the neutron angular distribution measurements are quite reasonable.

The high total yield of neutrons observed by Knox[13] can also be qualitatively explained by the values of the enlarged stripping cross sections without invoking contributions from the electric stripping, which appears to be negligible in comparison.

D. Comparison with Theory

Although it was expected that the nuclear transparency should allow some contribution to stripping from the central portion of the nucleus, that contribution cannot be calculated easily. However, a few simple considerations can give some ideas concerning the quantities measured in this experiment.

Let σ_S be the Serber stripping cross section, σ_D be the Dancoff electric stripping cross section, τ_S be the transparency factor for 90 Mev nucleons near the edge of the nucleus, τ be the transparency factor for 90 Mev nucleons which pass through the main body of the nucleus, and R be the nuclear radius. The total stripping cross section can then be roughly represented by

$$\sigma = \sigma_S + \sigma_S \tau_S + (\pi R^2 - \sigma_S) \tau + \sigma_D \qquad (37)$$

That is, σ_S is the cross section for the proton missing the nucleus, while the neutron hits the edge; $\sigma_S \tau_S$ is the cross section for the neutron missing the nucleus while the proton hits the edge, but traverses with probability τ_S; $(\pi R^2 - \sigma_S)$ is the probability that both the incident nucleons strike the nucleus, and, when multiplied by τ, gives the cross section for the proton emission.

As a rough approximation, we can take τ_s equal to unity; it is probably somewhat larger than τ. A value for τ can be inferred from the analysis of neutron scattering made by Fernbach, Serber and Taylor.[14] They find that the absorption cross sections for 90 Mev nucleons in beryllium and uranium are 0.55 and 0.88 of the geometric cross sections, respectively. This means that the respective transparency factors in these nuclei are 0.45 and 0.12, which lead to total stripping cross section values of approximately 0.33 barns for beryllium, and approximately 1.3 barns for uranium. Comparing these with the measured values, it would seem that while the agreement in the case of beryllium is excellent, this simple mechanism does not account for the high uranium value. If, on the other hand, the theory is roughly correct, the measurement implies a nuclear transparency of about 0.6 for uranium, which is clearly in disagreement with absorption cross section measurements. Thus, under either interpretation, a fundamental discrepancy exists which cannot be resolved with the present information concerning those processes which appear to be important in producing high energy charged secondaries by deuteron bombardment.

VII ACKNOWLEDGEMENTS

The author wishes to express his sincere gratitude to Professor A. C. Helmholz for his valuable guidance and support in all phases of the work. The assistance given by Dr. Walter E. Crandall in planning and executing the experiment, and the continued encouragement of Dr. C. M. Van Atta are gratefully acknowledged. Thanks are due to Dr. A. V. Shelton, Mr. D. A. Hicks, and Mr. G. P. Millburn for aid in carrying out the runs, and for the construction of equipment. The author is also indebted to Dr. Warren Heckrotte for enlightening discussions concerning the interpretation of the results. Finally, thanks are due to the members of the cyclotron crew, the accelerator technicians, and the electronics maintenance group whose combined efforts made the investigation possible.

This work was performed under the auspices of the Atomic Energy Commission.

VIII REFERENCES

1. N. Bohr, Nature 137, 344 (1936).
2. R. Serber, Phys. Rev. 72, 1008 (1947).
3. S. M. Dancoff, Phys. Rev. 72, 1017 (1947).
4. M. L. Goldberger, Phys. Rev. 72, 1269 (1948).
5. G. F. Chew and M. L. Goldberger, Phys. Rev. 77, 470 (1950).
6. S. T. Butler, Phys. Rev. 80, 1095 (1950).
7. C. E. Leith, Phys. Rev. 78, 89 (1950).
8. W. E. Crandall (private communication).
9. J. Hadley and H. York, Phys. Rev. 80, 345 (1950).
10. K. Strauch and J. A. Hofmann, Phys. Rev. 86, 563 (1952).
11. W. A. Aron, B. G. Hoffman, and F. C. Williams, AECU-663.
12. A. C. Helmholz, E. M. McMillan, and D. W. Sewell, Phys. Rev. 72, 1003 (1947).
13. W. J. Knox, Phys. Rev. 81, 687 (1951).
14. S. Fernbach, R. Serber, and T. B. Taylor, Phys. Rev. 75, 1352 (1949).

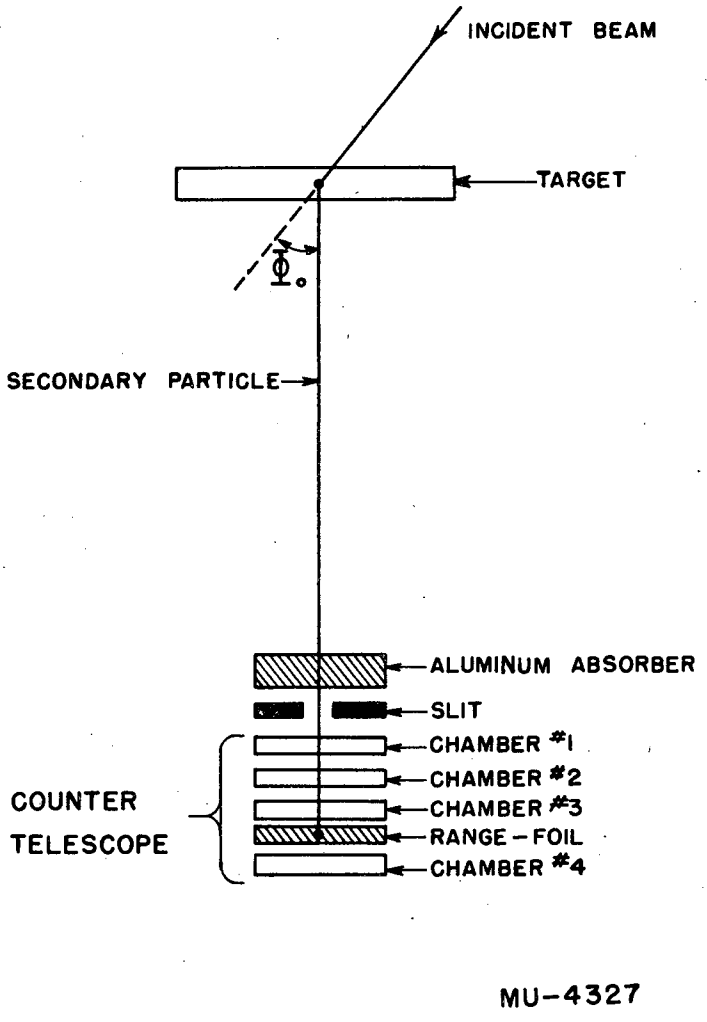

Figure 1

Schematic diagram of the four chamber proportional counter telescope.

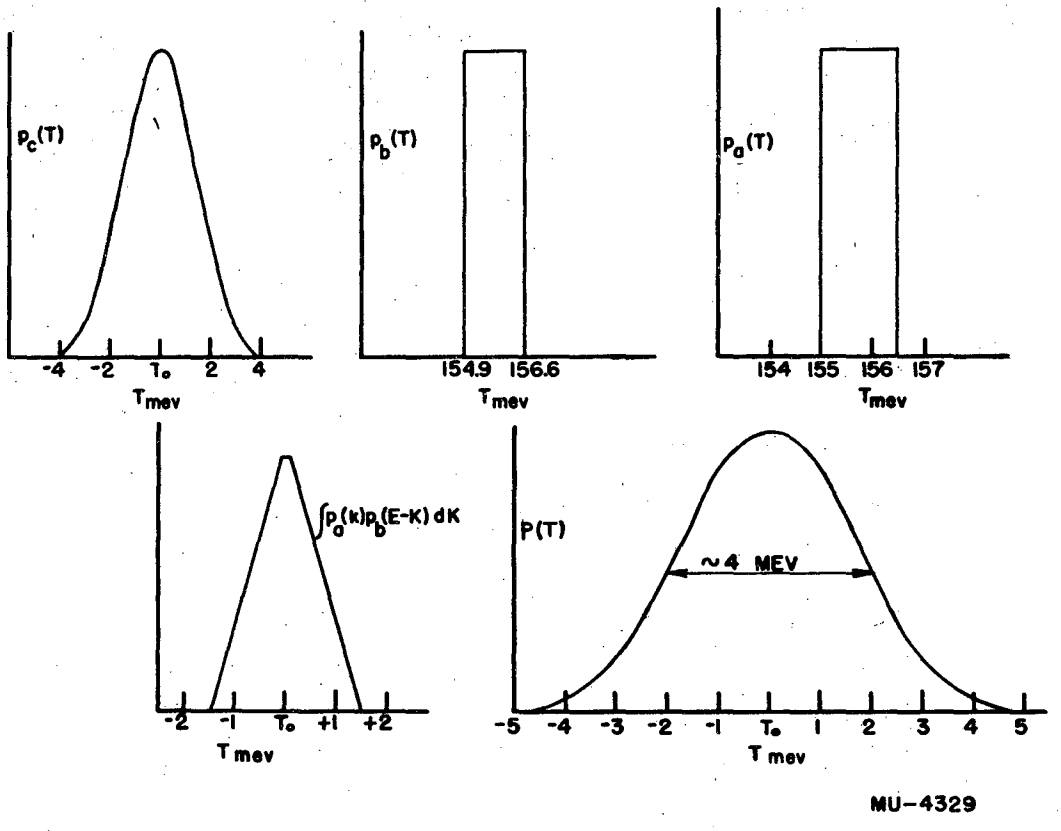

Figure 2

The energy resolution of the detector, as the fold of the several detector functions. The fold was integrated graphically.

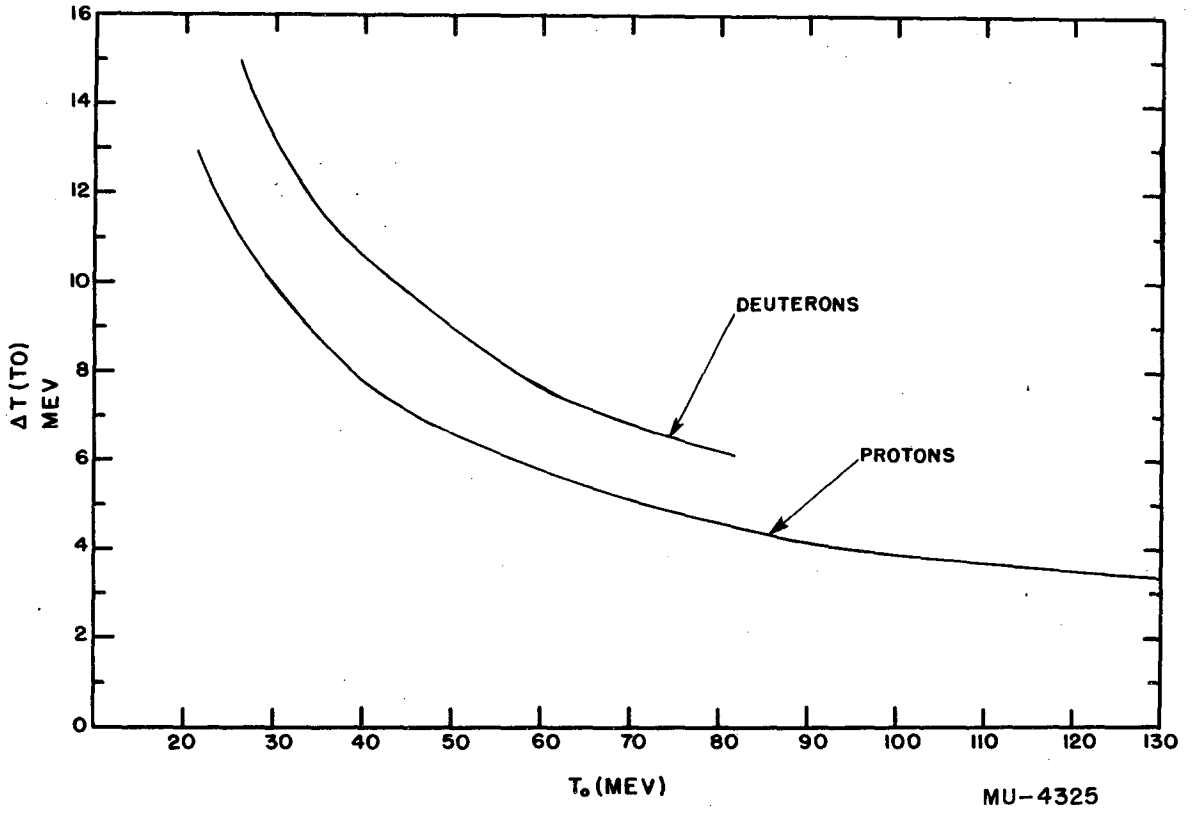

Figure 3

The integral of the detector energy resolution as a function of energy.

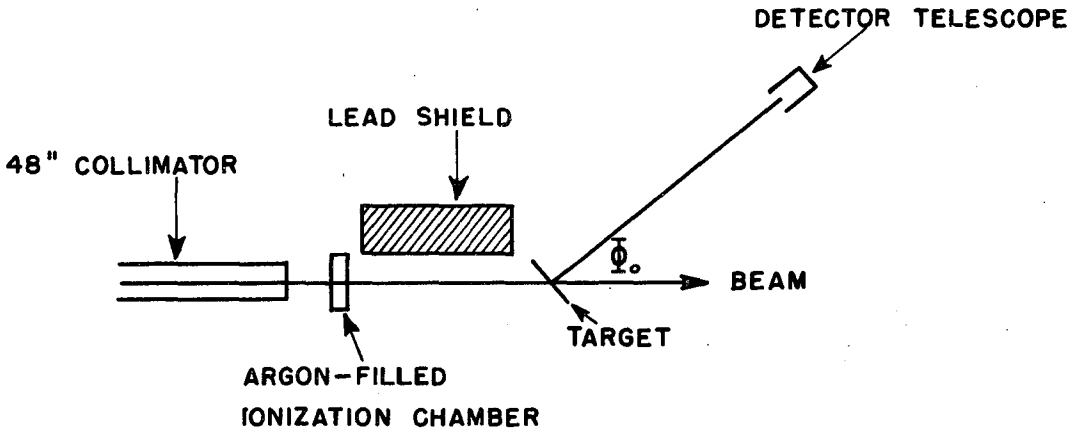

MU-4326

Figure 4

Schematic diagram of the experimental arrangement.

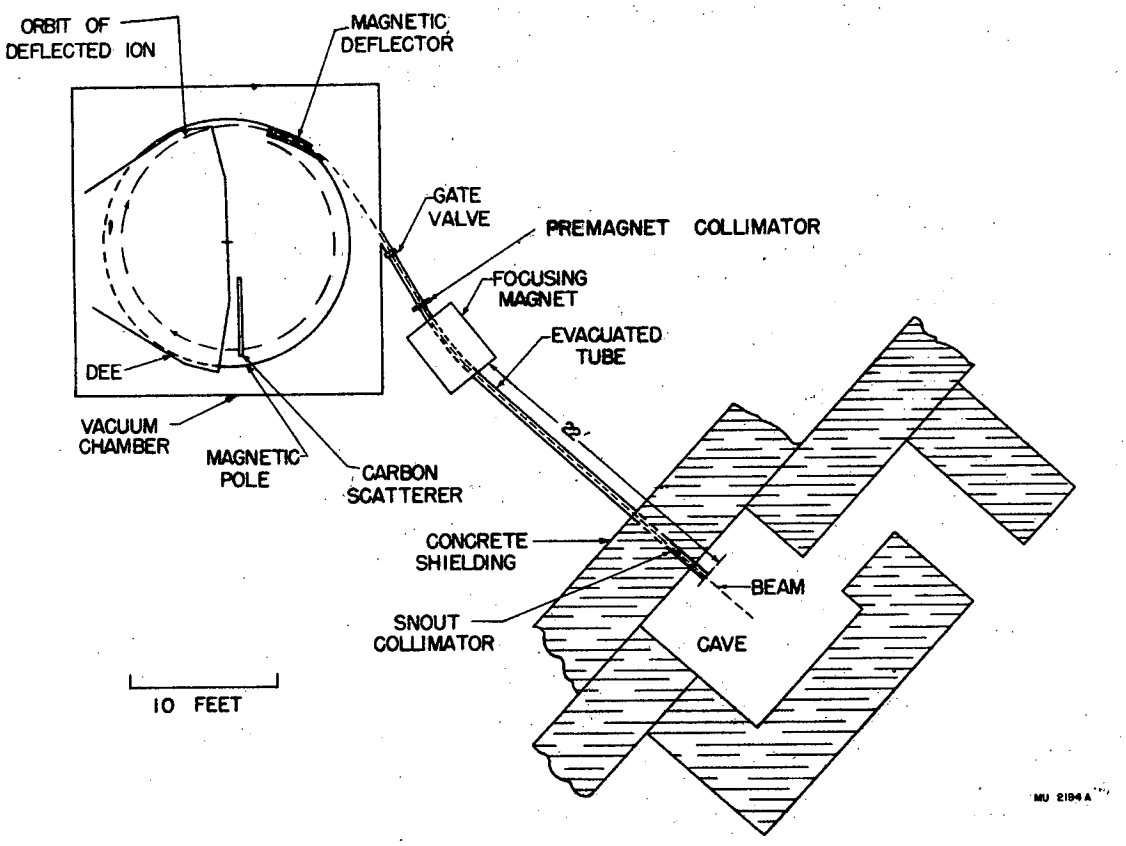

Figure 5

Schematic diagram of cyclotron and shielded enclosure.

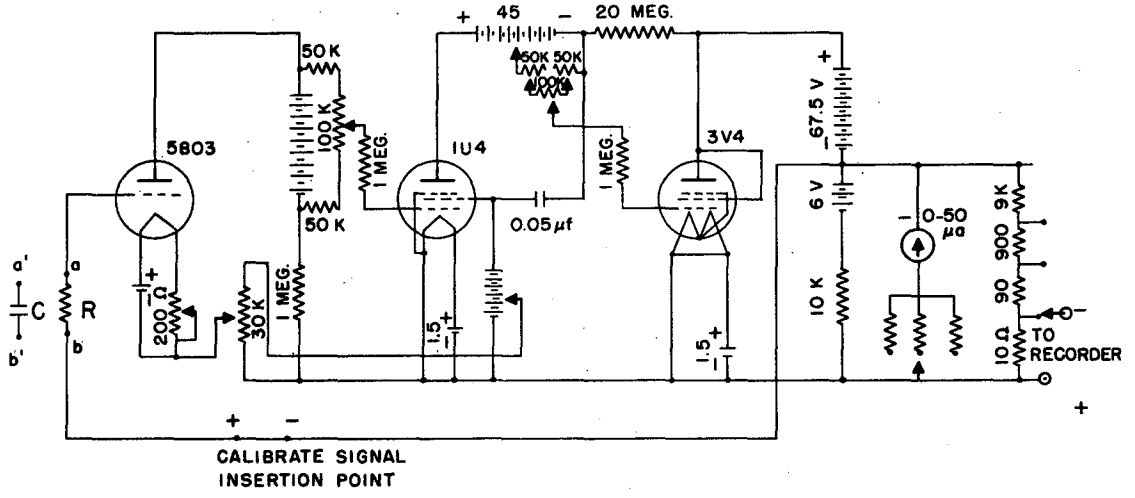

NOTE: "C" IS USED FOR INTEGRATING ELECTROMETER
"R" IS USED FOR CURRENT ELECTROMETER

MU3360

Figure 6

Simplified schematic diagram of the integrating electrometer circuit.

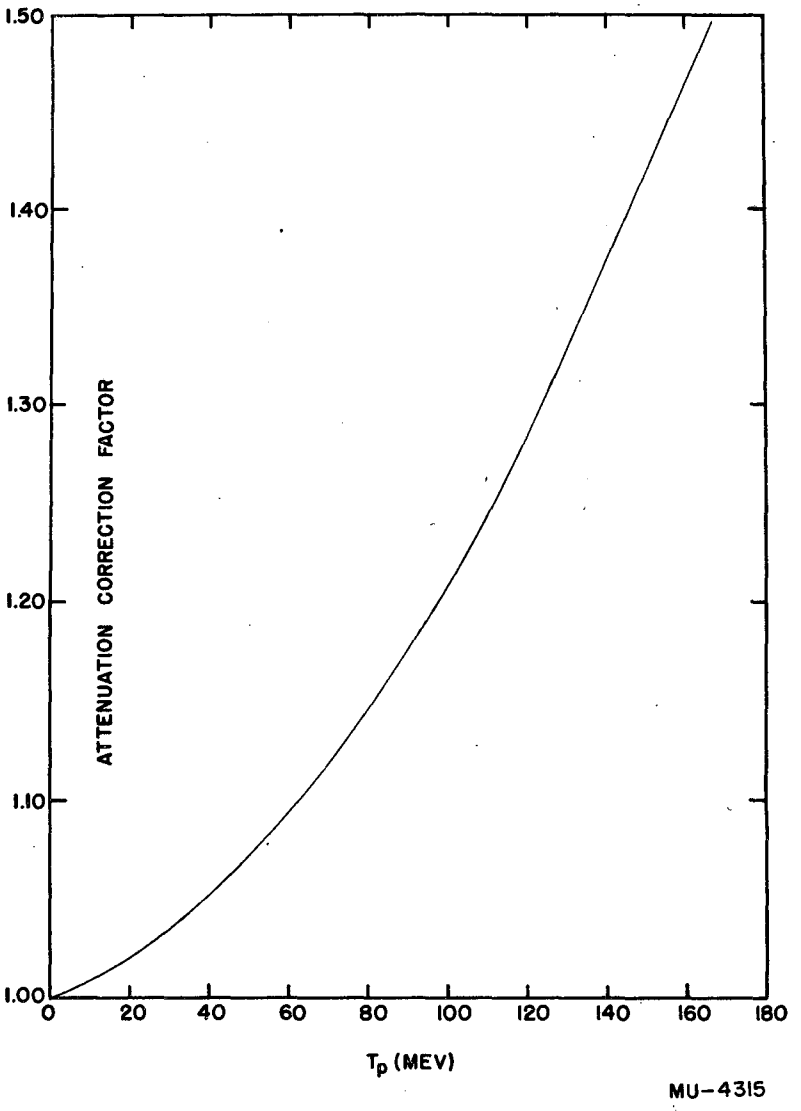

Figure 7

Proton attenuation correction as a function of proton energy.

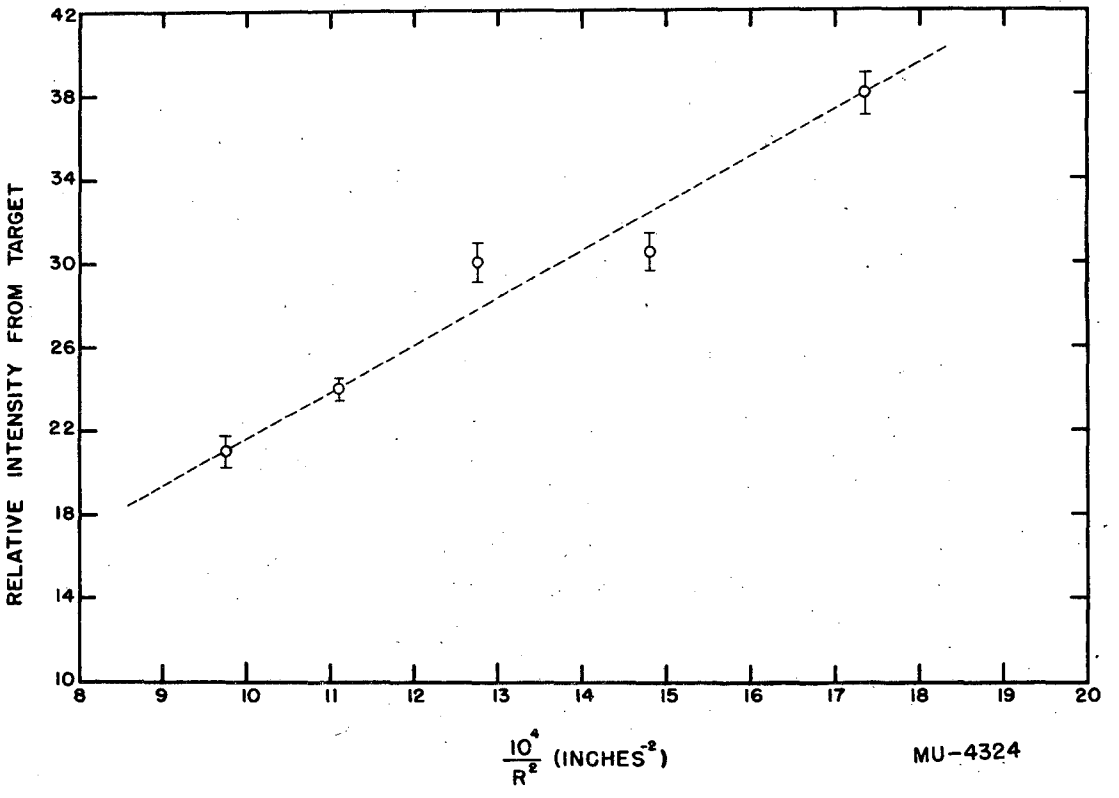

Figure 8

The relative detector counting rate as a function of the reciprocal of the square of the distance between target and detector slit.

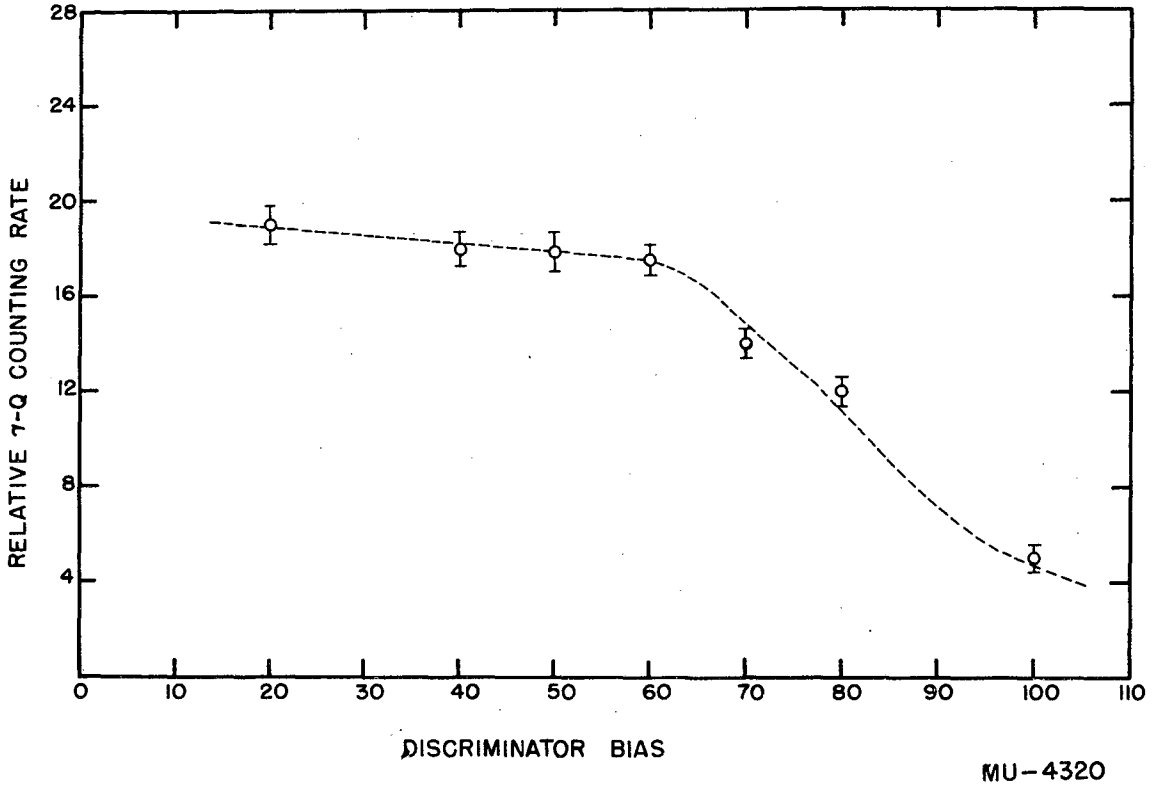

Figure 9

The relative detector counting rate as a function of the discriminator bias setting on the first three chambers.

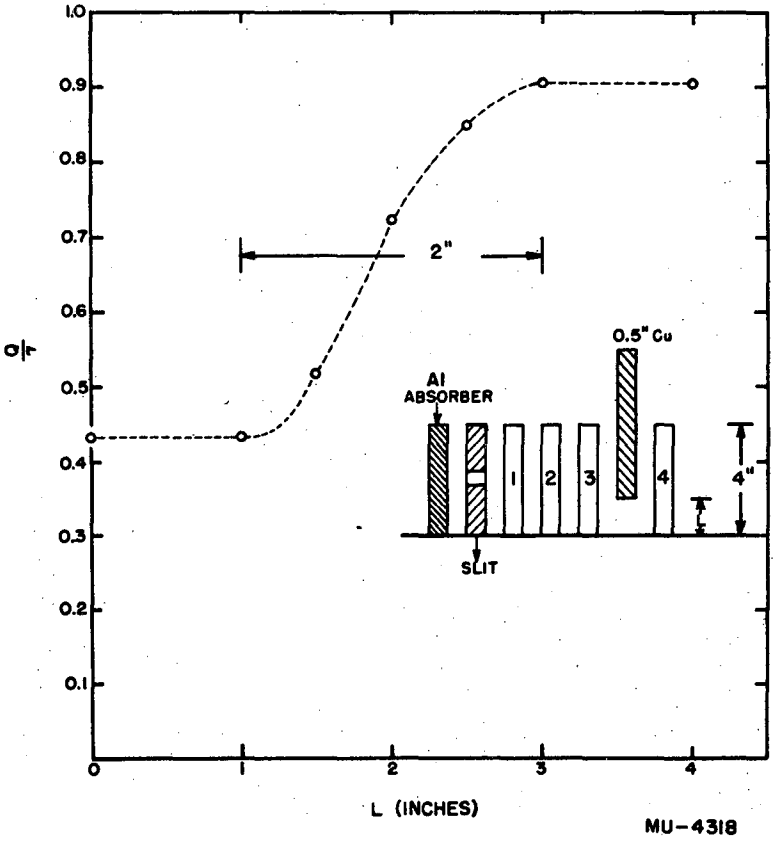

Figure 10

The relative detector counting rate as a function of the height of the shield between the third and fourth chambers.

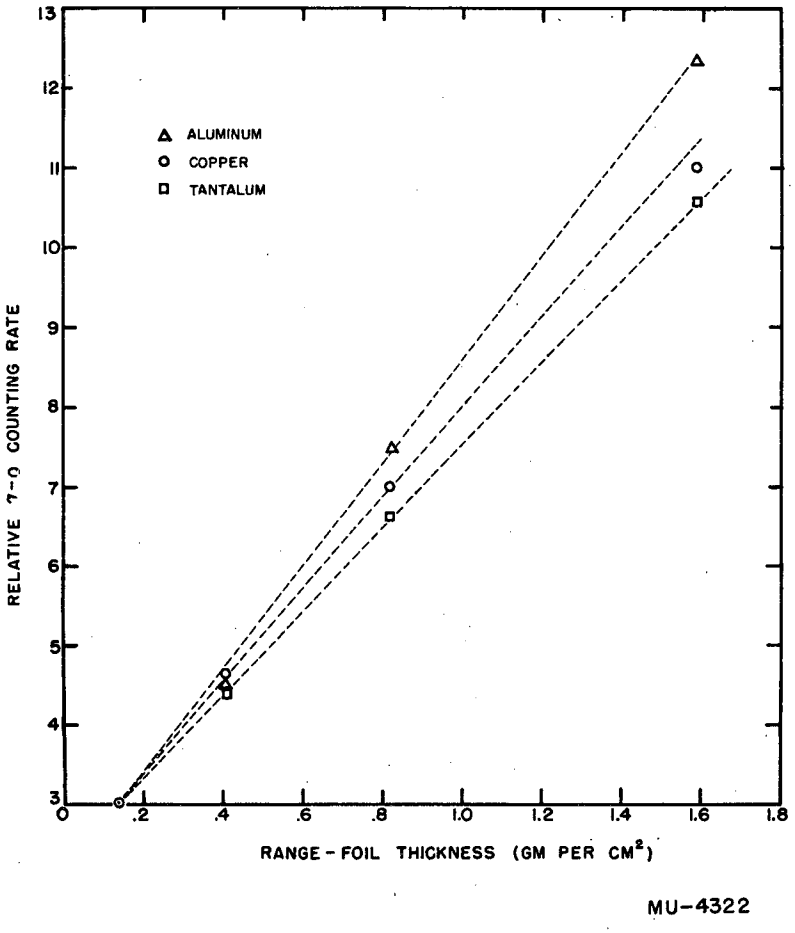

Figure 11

The relative detector counting rate as a function of range-foil thickness for aluminum, copper, and tantalum range-foils.

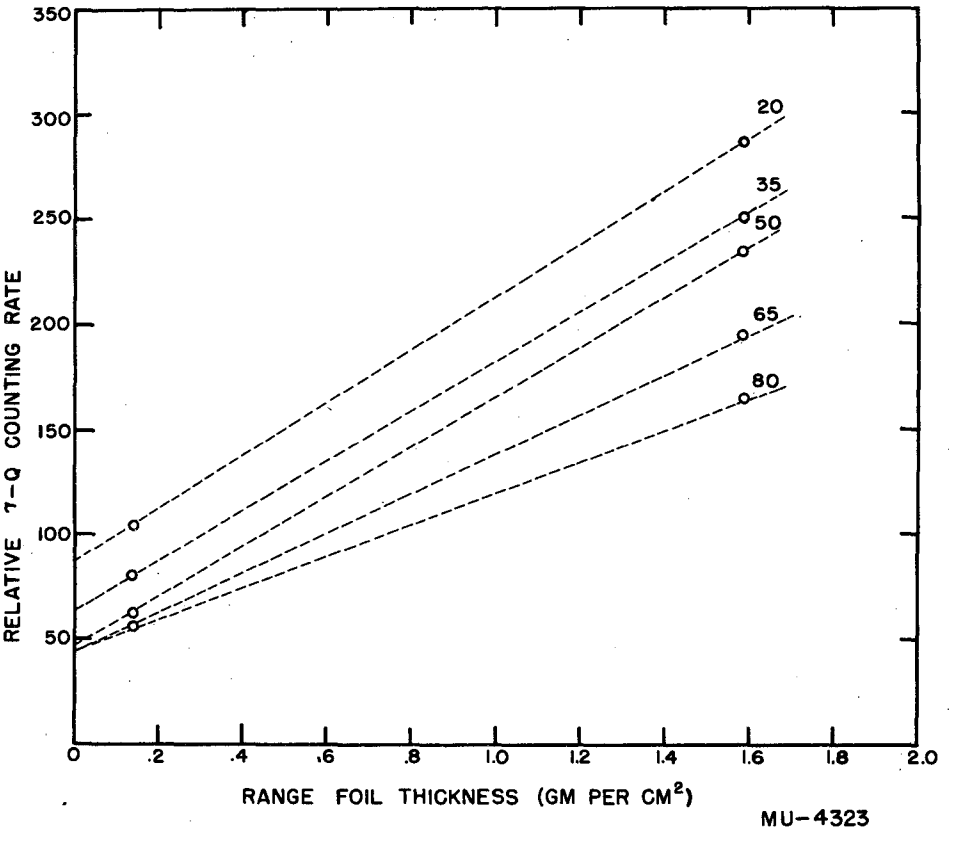

Figure 12

The relative detector counting rate for two different values of range-foil thickness as a function of the discriminator bias setting on the first three chambers.

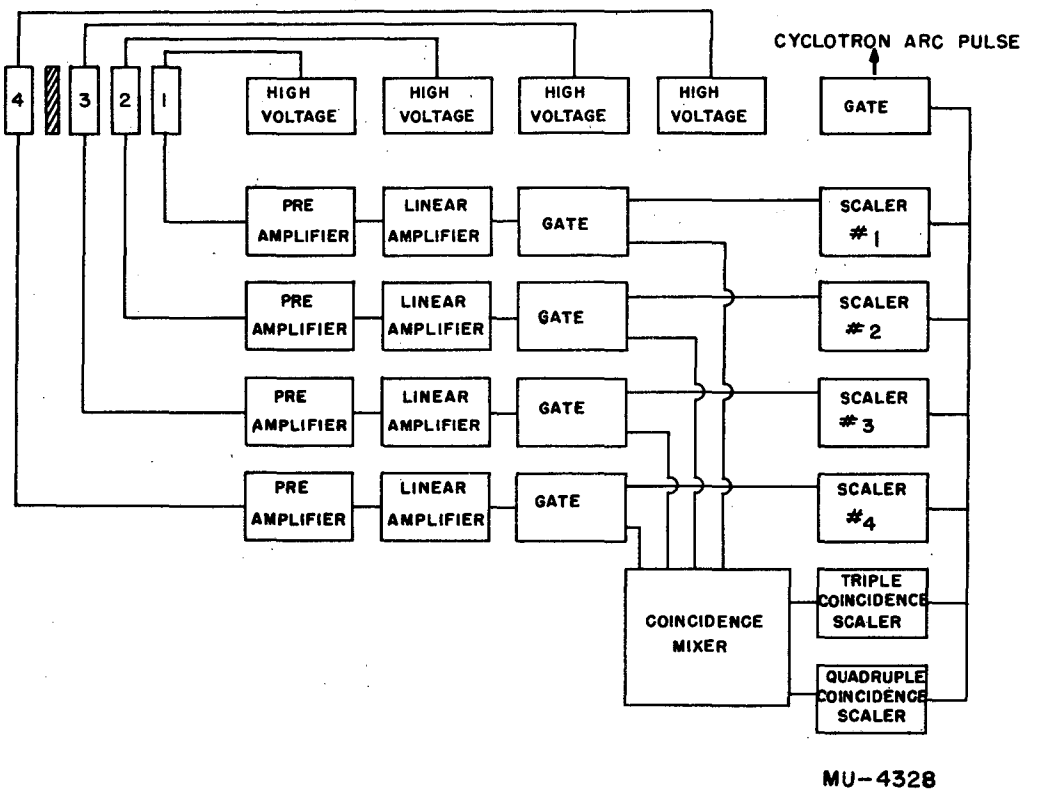

Figure 13

Block diagram of the electronics associated with the detector.

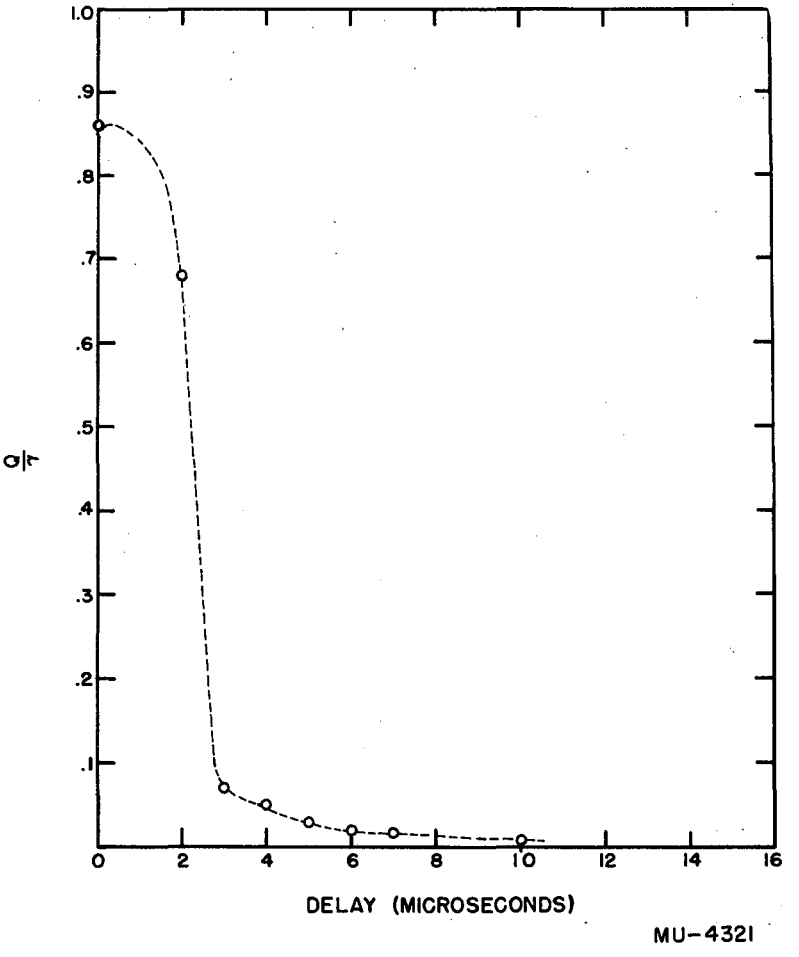

Figure 14

The relative detector counting rate as a function of the delay on the fourth chamber gate, measured with respect to the gates on the first three chambers.

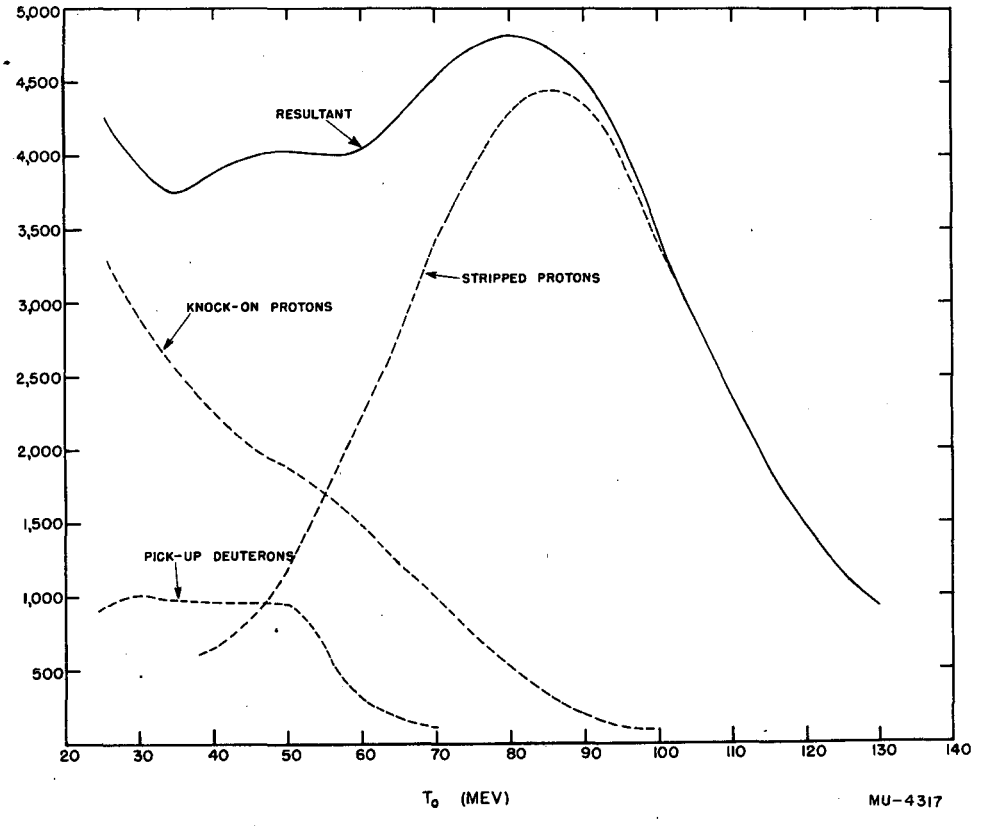

Figure 15

Example of the construction of a composite yield curve from its components. The case shown is for the carbon target at $\theta = 10^{\circ}$.

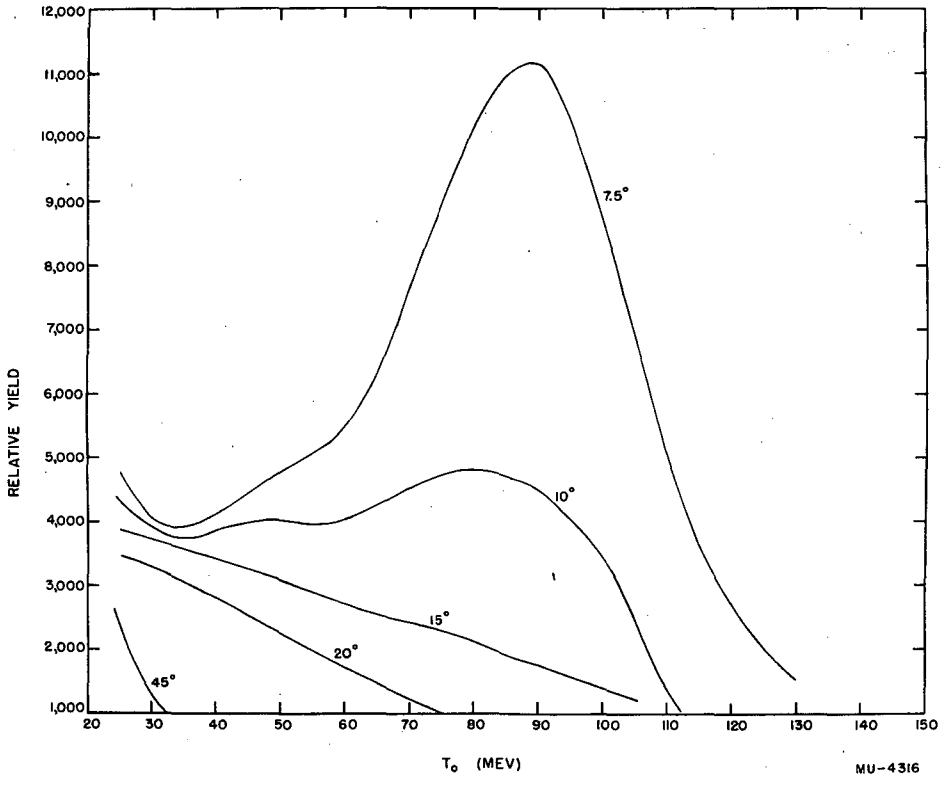

Figure 16

A complete set of composite curves for the angles investigated experimentally. The case shown is for the carbon target.

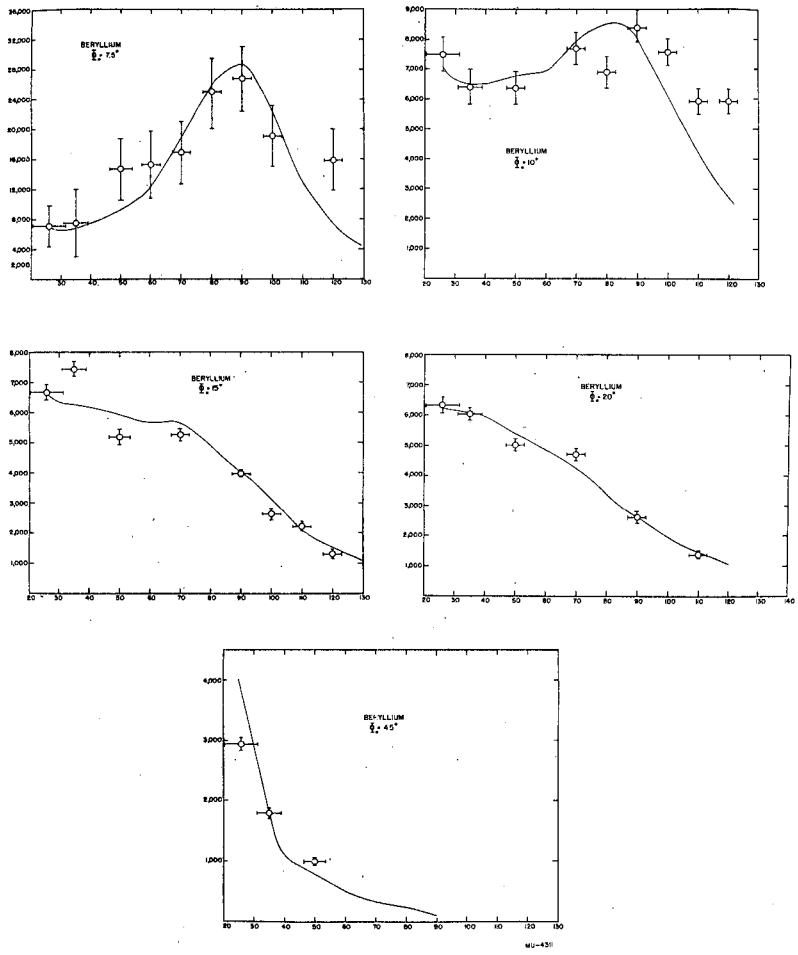

Figure 17

The energy distributions of secondary charged particles from a thin beryllium target at laboratory angles of 7.5°, 10°, 15°, 20°, and 45°. The abcissae are in Mev on the proton energy scale. The ordinates are in number of counts detected per microcoulomb of incident deuterons.

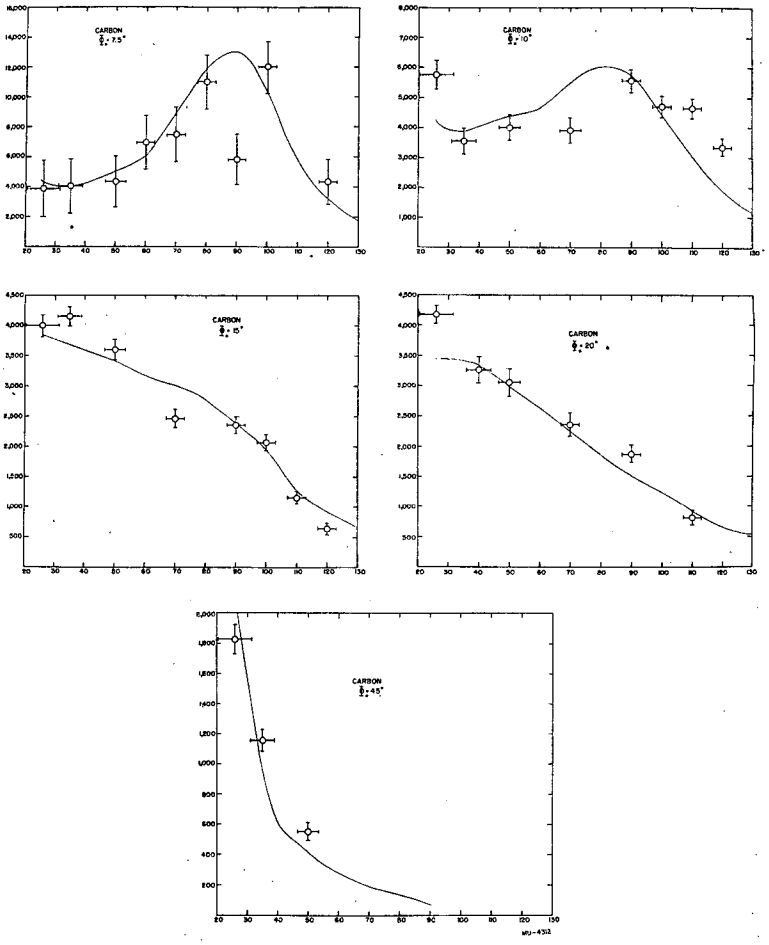

Figure 18

The energy distributions of secondary charged particles from a thin carbon target at laboratory angles of 7.5°, 10°, 15°, 20°, and 45°. The abcissae are in Mev on the proton energy scale. The ordinates are in number of counts detected per microcoulomb of incident deuterons.

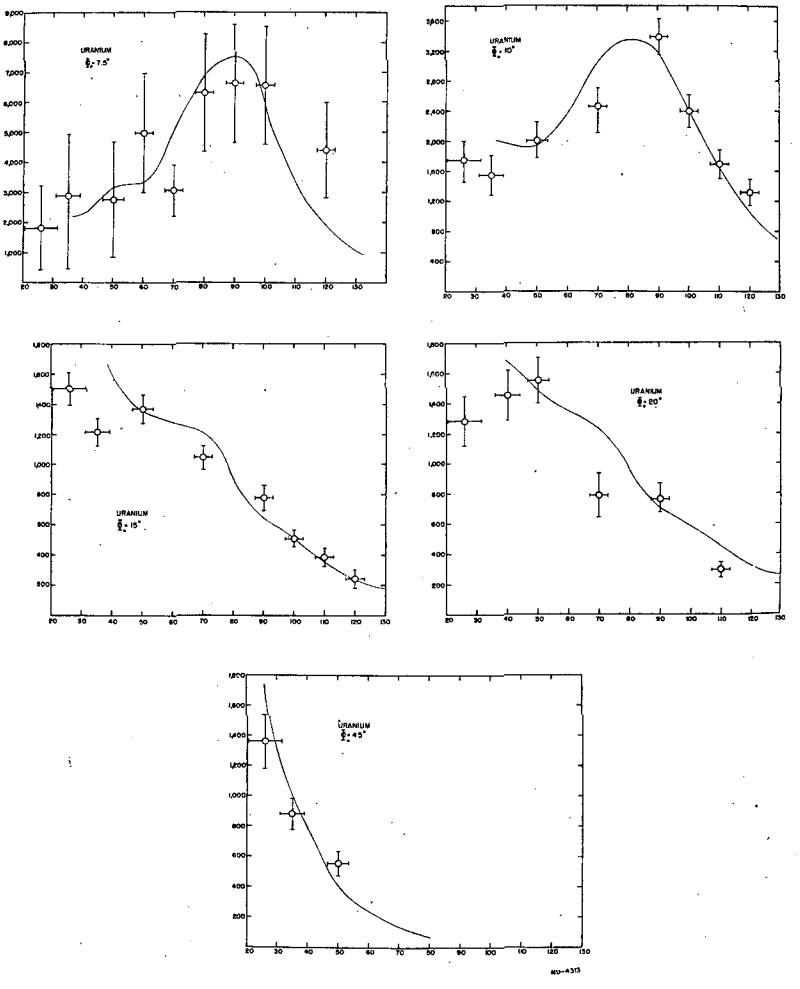

Figure 19

The energy distributions of secondary charged particles from a thin uranium target at laboratory angles of 7.5°, 10°, 15°, 20°, and 45°. The abcissae are in Mev on the proton energy scale. The ordinates are in number of counts detected per microcoulomb of incident deuterons.

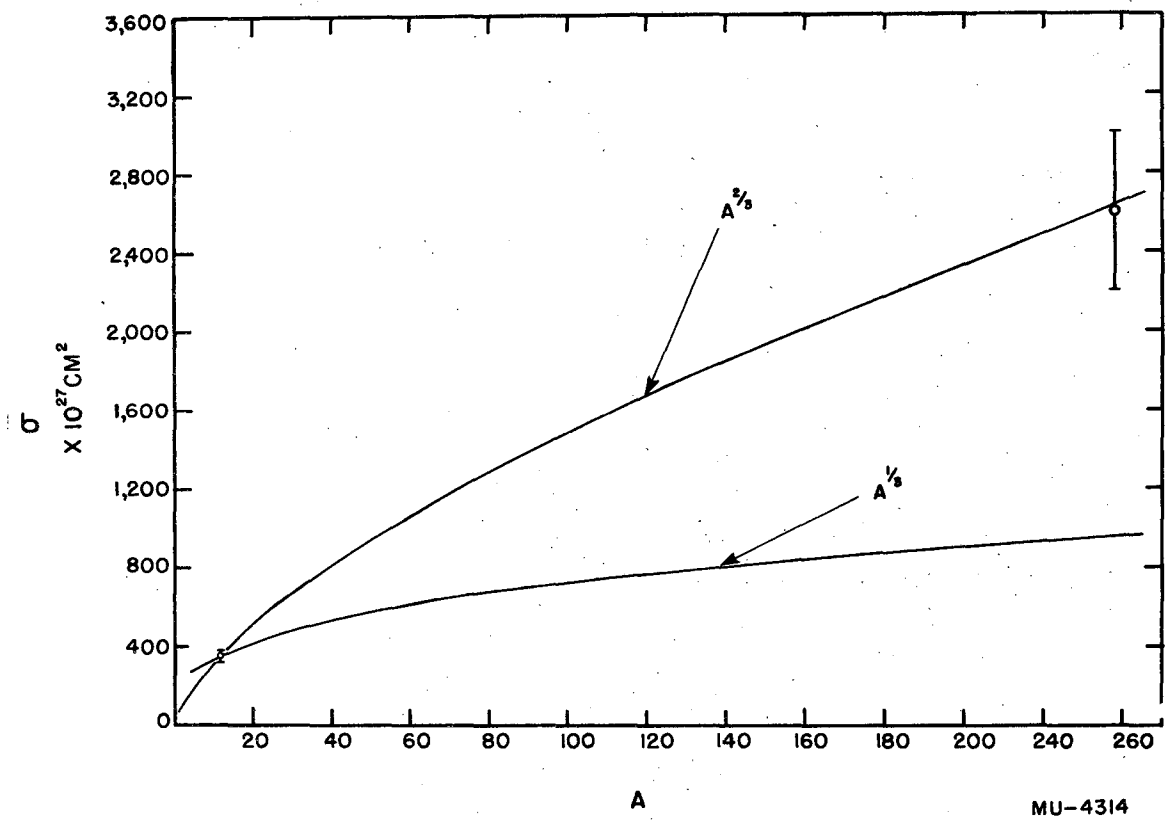

Figure 20

The enlarged stripping cross section as a function of atomic weight.

TABLE I

$$\Sigma = \iint \frac{d^2\sigma}{d\Omega\, dT}\, dT\, d\Omega = 2\pi C \int_0^{\infty}\int_0^{\pi} \frac{\sqrt{T_1}\,\sin\phi\, d\phi\, dT}{\left[\frac{\epsilon_d}{2} + T_0 + T_1 - 2\sqrt{T_1 T_0}\cos\phi\right]^2} = \frac{4\pi^2 C}{\sqrt{2\epsilon_d}}$$

TARGET	ANGLE	Σ	σ	
BE	7.5°	$.40\times10^{-24}$ cm^2	$.03\times10^{-24}$ cm^2	
	10°	.26	.02	
	15°	.34	.01	
	20°	.58	.05	$\bar{\Sigma} = 0.35 \pm 0.03 \times 10^{-24}$ cm^2
C	7.5°	.33	.06	
	10°	.36	.03	
	15°	.38	.02	
	20°	.64	.07	
U	7.5°	2.9	.8	
	10°	2.9	.1	$\bar{\Sigma} = 2.6 \pm 0.4 \times 10^{-24}$ cm^2
	15°	1.6	.2	
	20°	4.6	.7	

MU-4319

The measured cross sections and their weighted averages.